

1 **A dataset of energy, water vapor and carbon exchange observations**  
2 **in oasis-desert areas from 2012 to 2021 in a typical endorheic basin**

3  
4 Shaomin Liu<sup>1</sup>, Ziwei Xu<sup>1</sup>, Tao Che<sup>2</sup>, Xin Li<sup>3</sup>, Tongren Xu<sup>1</sup>, Zhiguo Ren<sup>2</sup>,  
5 Yang Zhang<sup>2</sup>, Junlei Tan<sup>2</sup>, Lisheng Song<sup>4</sup>, Ji Zhou<sup>5</sup>, Zhongli Zhu<sup>1</sup>, Xiaofan  
6 Yang<sup>1</sup>, Rui Liu<sup>6</sup>, Yanfei Ma<sup>7</sup>

7 *Correspondence to:* Shaomin Liu (smliu@bnu.edu.cn), Ziwei Xu (xuzw@bnu.edu.cn)

8  
9 <sup>1</sup>State Key Laboratory of Earth Surface Processes and Resource Ecology, Faculty of Geographical  
10 Science, Beijing Normal University, Beijing 100875, China

11 <sup>2</sup>Northwest Institute of Eco-Environment and Resources, Chinese Academy of Sciences, Lanzhou  
12 730000, China

13 <sup>3</sup>National Tibetan Plateau Data Center, State Key Laboratory of Tibetan Plateau Earth System and  
14 Resources Environment, Institute of Tibetan Plateau Research, Chinese Academy of Sciences,  
15 Beijing 100101, China

16 <sup>4</sup>Key Laboratory of Earth Surface Processes and Regional Response in the Yangtze-Huaihe River  
17 Basin, School of Geography and Tourism, Anhui Normal University, Wuhu 241000, China;

18 <sup>5</sup>School of Resources and Environment, University of Electronic Science and Technology of China,  
19 Chengdu 611731, China

20 <sup>6</sup>Institute of Urban Study, School of Environmental and Geographical Sciences (SEGS), Shanghai  
21 Normal University, Shanghai 200234, China

22 <sup>7</sup>Hebei Technology Innovation Centre for Remote Sensing Identification of Environmental Change,  
23 Hebei Key Laboratory of Environmental Change and Ecological Construction, School of  
24 Geographical Sciences, Hebei Normal University, Shijiazhuang 050024, China

29 **Abstract:**

30 Oases and deserts generally act as a landscape matrix and mosaic in arid/semiarid  
31 regions. The significant difference of thermal and dynamic characteristics between  
32 oasis and desert surface will result in oasis-desert interaction. That is, the interaction  
33 between oasis and desert system through the exchange of momentum, energy, water  
34 and carbon, which can lead to a series of microclimate effects that affect the structure  
35 of the atmospheric boundary layer, changes of carbon sources/sinks in oasis and the  
36 local ecological environment. Therefore, studying water, heat and carbon exchange is  
37 significant for achieving the goals of carbon peaking and carbon neutrality in oasis-  
38 desert areas and supporting the ecological security and sustainable development of  
39 oases. To monitor energy, water vapor and carbon exchange between the land surface  
40 and atmosphere, a land surface process integrated observatory was established in the  
41 oasis-desert area in the middle and lower reaches of the Heihe River Basin, the 2<sup>nd</sup>  
42 largest endorheic basin in China. In this study, we present a suite of observational  
43 datasets in artificial and natural oases-desert systems, which consist of long-term energy,  
44 water vapor, carbon/methane fluxes, and auxiliary data involving hydrometeorology,  
45 vegetation and soil parameters from 2012 to 2021. Half-hourly turbulent flux data were  
46 acquired by an eddy covariance system and scintillometer. The hydrometeorological  
47 data, including radiation, soil heat flux and soil temperature profile, gradient of air  
48 temperature/humidity and wind speed/direction, air pressure, precipitation and soil  
49 moisture profiles, were observed from automatic weather stations with a 10-minute  
50 average period as well as the groundwater table data. Moreover, vegetation and soil

51 parameters were also supplemented in the datasets. Careful data processing and quality  
52 control are implemented during data production, including data collection, processing,  
53 archiving and sharing. The current datasets can be used to explore the water-heat-carbon  
54 process and its influence mechanism, calibrate and validate related remote sensing  
55 products, simulate energy, water vapor and carbon exchange in oasis and desert areas,  
56 and provide references and representatives for other similar artificial and natural oases  
57 along the Silk Road. The datasets are available from the National Tibetan Plateau Third  
58 Pole Environment. The dataset can be assessed from  
59 <https://doi.org/10.11888/Terre.tpdc.300441> (Liu et al., 2023).

60

## 61 **1. Introduction**

62 Arid and semiarid regions represent approximately 30% of the global terrestrial surface  
63 area (Dregne, 1991; Scanlon et al., 2006), and dryland expansion occurs under climate  
64 change, especially in developing countries (Huang et al., 2015). This proportion is much  
65 higher in China, as (semi)arid regions account for approximately 47% of its terrestrial  
66 surface (Zhang et al., 2016a; Mao et al., 2018). An oasis is a unique ecological  
67 landscape in arid and semiarid areas, which is not only the core of its ecological  
68 environment but also the foundation of its economic development, especially in western  
69 China, which has been an important part of the ‘Silk Road’ since ancient times. Oases  
70 with less than 10% of the total area of arid regions support more than 90% of the  
71 population in the arid regions of China (Chu et al., 2005; Li et al., 2016; Zhou et al.,  
72 2022). The main geomorphologic feature is a wide sandy desert or Gobi (gravel desert),

73 interspersed with many oases of different sizes and shapes in the middle and lower  
74 reaches of a typical endorheic basin in Northwest China (Cheng et al., 1999). The water  
75 from upstream is the link connecting these ecosystems, and the oasis is the place where  
76 human beings live. The oasis areas are now 3.3 times larger than those in the early  
77 1950s in the region of northwestern China (Zhang et al., 2018). The oasis-desert system  
78 plays a crucial role in maintaining a stable ecological environment and agricultural  
79 productivity (Zhang and Zhao, 2015). However, inland river basins in arid and semiarid  
80 areas are facing the crisis of ecological environment degradation, such as the drying up  
81 of rivers and lakes, the degradation of natural vegetation, the intensification of land  
82 desertification and the frequent occurrence of dust storms, especially in many inland  
83 river basins westward along the Silk Road, such as the Tarim River Basin (Zhao et al.,  
84 2013), Aral Sea Basin (Stanev et al., 2004; Crétaux et al., 2009), and Lake Urmia Basin  
85 (Stone, 2015). Therefore, it is critical to maintain the balance between the oasis and  
86 desert systems to achieve the goal of sustainable oasis development.

87 The particularity of the underlying surface in the oasis-desert area, e.g., the irrigation  
88 cropland, riparian forest, sandy vegetation, seasonal snow and frozen soil, makes the  
89 study of land-atmosphere interactions complex and needs comprehensive consideration  
90 in such heterogeneous underlying surfaces. The dynamic and thermal characteristics of  
91 the underlying surface of the oasis and the desert are significantly different, and the  
92 oasis and desert systems interact and influence each other through momentum, energy,  
93 water vapor and carbon exchange. Thus, the oasis-desert interaction will affect the  
94 structure of the atmospheric boundary layer and the local ecological environment.

95 Additionally, under the influence of weather conditions, the oasis-desert interaction  
96 results in the local circulation between oasis and desert and airflows form dynamic and  
97 thermal inner boundary layer within the oasis (Cheng et al., 2014). These can lead to  
98 the local microclimate characteristics of the oasis-desert area (Liu et al., 2020), such as  
99 the wind shield effect and cold-wet island effect of the oasis, the humidity inversion  
100 effect within the surrounding desert, and oasis carbon sources/sinks. These  
101 microclimate effects play an important role in the self-sustaining and development of  
102 oasis systems. Understanding the basic characteristics of energy, water vapor and  
103 carbon exchange in oasis-desert ecosystems is important for achieving the goals of  
104 carbon peaking and carbon neutrality in the oasis-desert area and supporting ecological  
105 security and sustainable development of the oasis.

106 Extensive studies have investigated energy, water vapor and carbon exchange in  
107 oasis-desert areas based on field and remote sensing observations (Taha et al., 1991;  
108 Potchter et al., 2008; Xue et al., 2019; Wang et al., 2019; Zhou et al., 2022) and  
109 numerical simulations (Chu et al., 2005; Meng et al., 2009; Georgescu et al., 2011; Liu  
110 et al., 2020). Li et al. (2016) provided a complete sketch map of oasis and desert  
111 interactions based on previous studies, including the oasis cold and wet island effect,  
112 oasis wind shield effect (oasis effect), and air humidity inversion effect within the  
113 surrounding desert (desert effect), which are important for the stability and  
114 sustainability of the oasis-desert ecosystem (Liu et al., 2020). In addition, the oasis-  
115 desert areas located in semiarid regions were found to be carbon sinks by previous  
116 researchers (Tagesson et al., 2016; Wang et al., 2019), which can significantly affect

117 the carbon balance of arid regions and play an increasingly important role within the  
118 global carbon cycle.

119 The Heihe River Basin (HRB), the second largest endorheic basin in China, is  
120 characterized by artificial oases and natural oases in the middle and lower reaches,  
121 respectively. Several experiments have been conducted in these oasis-desert areas, e.g.,  
122 the Heihe River Basin Field Experiment (HEIFE) from 1990 to 1992 to conduct  
123 comprehensive studies of atmosphere–land surface interactions over the Zhangye oasis  
124 and desert area in the middle reaches of the HRB (Wang et al., 1992), the Jinta  
125 experiment from 2005 and 2008 to focus on the energy and water exchange and the  
126 atmospheric boundary over the Jinta oasis and desert area in the middle reaches of the  
127 HRB (Wen et al., 2012), the oasis-desert area in the middle reaches and mountainous  
128 area in upper reaches of watershed allied telemetry experimental research (WATER)  
129 and the subsequent HiWATER (oasis-desert area in the middle and lower reaches and  
130 mountainous area in upper reaches) to be a comprehensive simultaneous satellite–  
131 airborne–ground observations eco-hydrological experiment (Li et al., 2009, 2013).  
132 Thereafter, a multielement, multiscale, networked, and elaborate integrated observatory  
133 network was established in the oasis-desert area in the middle and lower reaches and  
134 mountainous area in upper reaches of the HRB since 2007 and completed in 2013 (Liu  
135 et al., 2018). A quantitative understanding of the energy, water vapor and carbon  
136 exchange in oasis-desert areas is crucial for recognizing the oasis-desert interactions  
137 and is significant for protecting the ecological stability and socioeconomic development  
138 of oases, and long-term observations are indispensable. The observations and research

139 findings from the oasis-desert area in the HRB will serve as references and  
140 representatives for other similar artificial and natural oases along the Silk Road. To  
141 achieve the aforementioned objective, observations should be continuously conducted,  
142 and a high-quality dataset should be obtained.

143 In this paper, the integrated observatory network of the artificial and natural oasis-  
144 desert areas in the middle and lower reaches in the HRB are introduced first, and the  
145 observations characterizing the energy, water vapor and carbon exchange are detailed  
146 explicated, which provides a 10-year dataset. Specifically, the spatial distribution and  
147 design of the observation sites are summarized in Section 2. Section 3 describes the  
148 data processing and quality control procedures. In Section 4, the energy, water vapor  
149 and carbon fluxes and related auxiliary parameters are introduced in detail. The data  
150 availability is documented in Section 5, and the conclusions are summarized in Section  
151 6. This dataset can be used for comprehensive understanding of energy, water vapor  
152 and carbon exchange in oasis-desert areas, and validating simulation results and remote  
153 sensing products of energy, water vapor and carbon fluxes in oasis-desert areas.

## 154 **2. A land surface process integrated observatory network in the oasis-desert area** 155 **of the HRB**

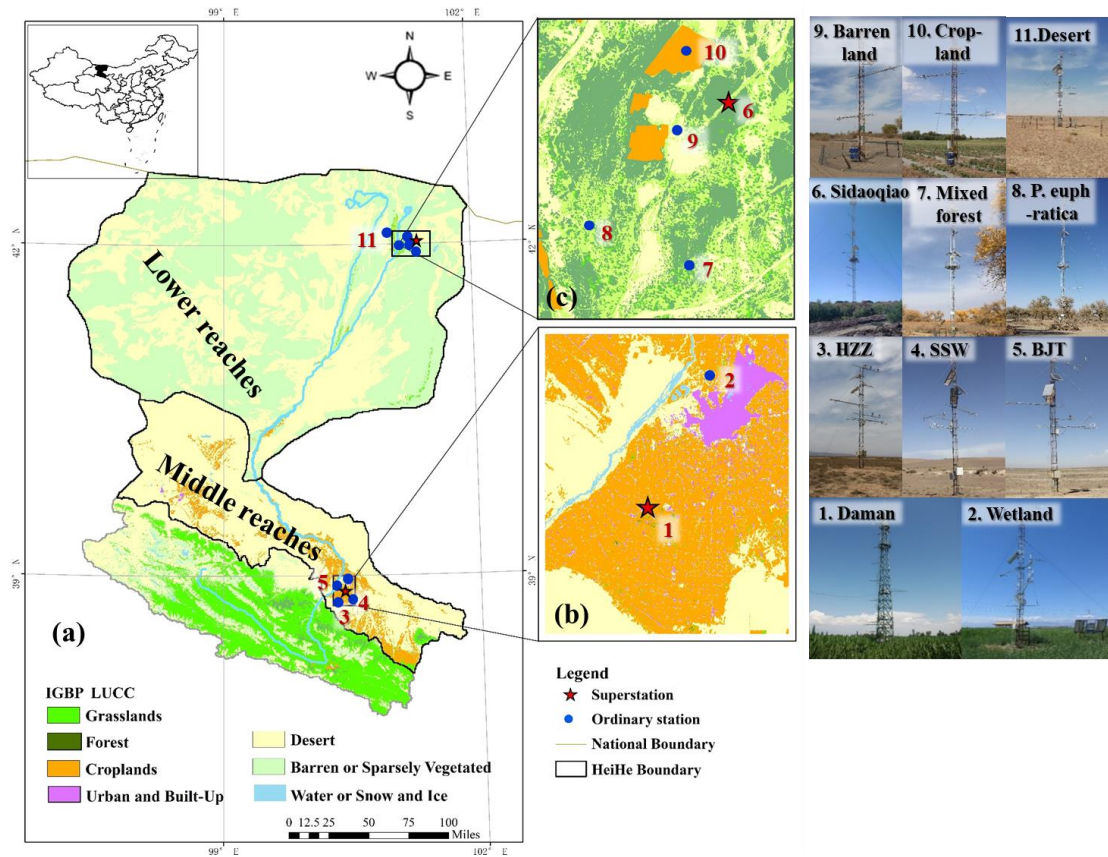
### 156 **2.1 Study area description**

157 The study areas are the middle and lower reaches of the HRB, which are located in  
158 the arid regions of western China, provided by water from the typical cryosphere of the  
159 upper reaches. In the upper reaches, glaciers, snow cover and frozen ground is widely

160 distributed and snowfall could occur in any season (elevation >3800 m). The typical  
161 snow depth is 15-30 cm with a duration of 90-120 days in the snow-covered regions  
162 (Che et al., 2012; Che et al., 2019). The middle reaches, typical of the artificial oasis-  
163 desert system in Zhangye City, the largest oasis in the Hexi Corridor, cover an area of  
164 29,717 km<sup>2</sup> with an oasis area of 5,560 km<sup>2</sup>, while the lower reaches in Ejina Banner  
165 have a natural oasis-desert system covering an area of 85,678 km<sup>2</sup> with an oasis area of  
166 1,130 km<sup>2</sup> (Fig. 1). Among the oases, agricultural oases can be traced to the history of  
167 more than 2000 years. The annual average air temperature was 7.29 °C and 9.75 °C,  
168 and the annual accumulated precipitation was 184.83 mm and 37.31 mm (1979-2018)  
169 in the middle and lower reaches, respectively.

170 Eleven land surface fluxes and meteorological stations have been established in these  
171 regions since 2012 with two superstations and eleven ordinary stations (Table 1; Section  
172 2.2), specifically two oasis stations and three desert stations in the middle reaches and  
173 five oasis stations and one desert station in the lower reaches.





174

175 Fig. 1. The middle and lower reach observation systems in the HRB. (a: Heihe River

176 basin; b: Stations in the Zhangye artificial oasis-desert area in the middle reaches; c:

177 Stations in the Ejina natural oasis area in the lower reaches)

178

Table 1. Station information in the middle and lower reaches of the HRB

ID	Name	Longitude (°, E)	Latitude (°, N)	Elevation (m)	Land Cover	Duration	Location
1	Daman	100.37	38.86	1556	Maize	May 2012- present	Oasis in midstream, superstation
2	Zhangye Wetland	100.45	38.98	1460	Wetland mainly reed	June 2012- present	Oasis in midstream, ordinary station
3	Huazhaizi Desert Steppe	100.32	38.77	1731	<i>Kalidium foliatum</i>	June 2012- present	Desert in midstream, ordinary station
4	Shenshawo Sandy Desert	100.49	38.79	1594	Sandy	June 2012- Apr.2015	Desert in midstream, ordinary station
5	Bajitan Gobi	100.30	38.92	1562	Reaumuria	May 2012- Apr.2015	Desert in midstream, ordinary station
6	Sidaoqiao	101.14	42.00	873	<i>Tamarix</i>	July 2013-	Oasis in downstream,

						present	superstation
7	Mixed Forest	101.13	41.99	874	<i>Populus euphratica and Tamarix</i>	July 2013-present	Oasis in downstream, ordinary station
8	Populus euphratica	101.12	41.99	876	<i>Populus euphratica</i>	July 2013-Apr.2016	Oasis in downstream, ordinary station
9	Barren Land	101.13	42.00	875	Bare land	July 2013-Mar.2016	Oasis in downstream, ordinary station
10	Cropland	101.13	42.00	875	Melon	July 2013-Nov.2015	Oasis in downstream, ordinary station
11	Desert	100.99	42.11	1054	Reaumuria	Apr.2015-present	Desert in downstream, ordinary station

## 179 2.2 Observation systems

### 180 2.2.1 Artificial oasis and desert areas in the middle reaches

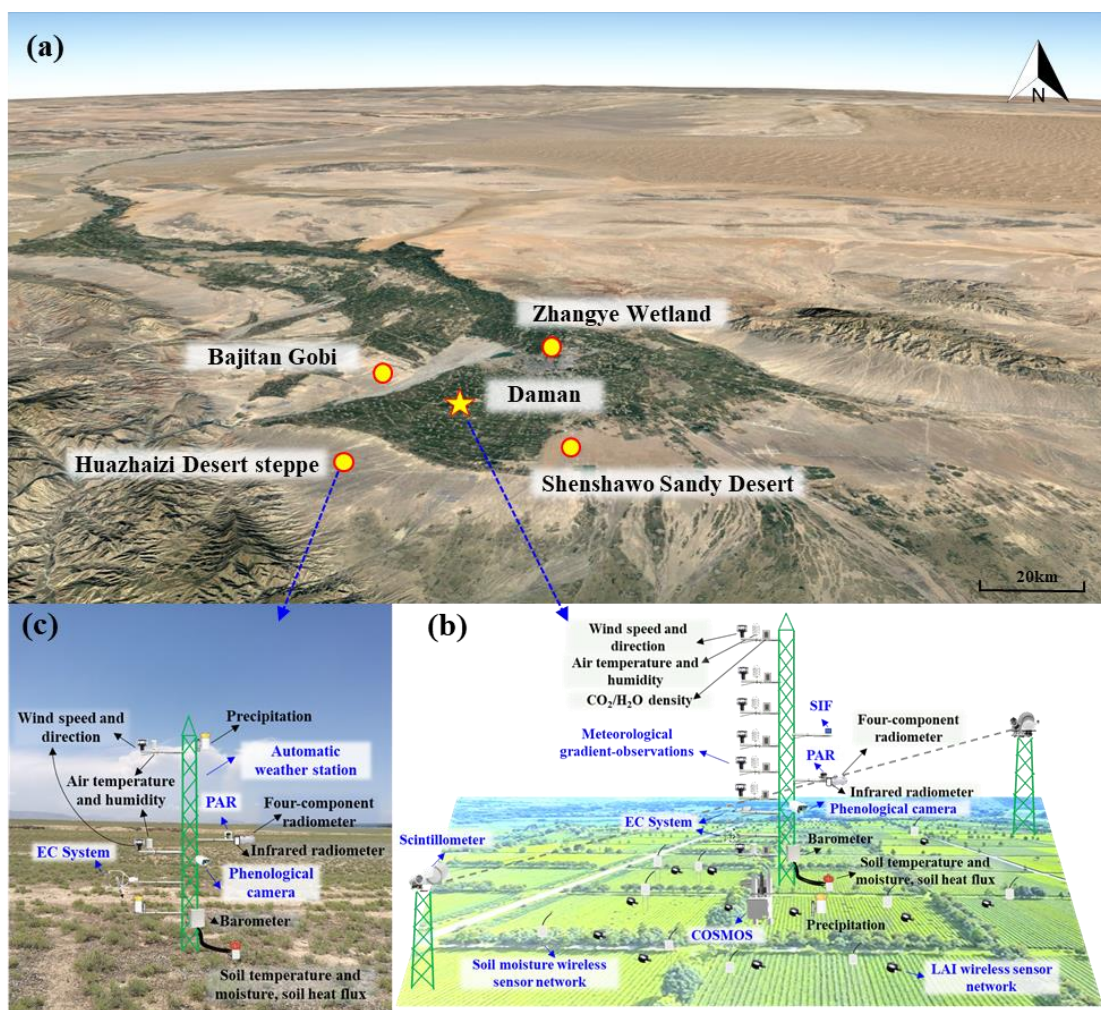
181 The middle reaches are located in the Zhangye oasis in Zhangye City of Gansu  
182 Province, and the primary underlying surfaces include cropland (maize), shelterbelt,  
183 orchard, residential area and wetland (reed) in the oasis and sandy desert, desert steppe  
184 (*Kalidium foliatum*), and the Gobi Desert (Reaumuria) in the surrounding desert. Five  
185 stations (one superstation and four ordinary stations) were established in these surfaces,  
186 which are representative of the main underlying surface types within the oasis-desert  
187 area in the middle reaches of the HRB.

188 There is one superstation (maize and shelterbelt) and one ordinary station (wetland  
189 and reed) in the Zhangye oasis surrounding three ordinary stations in the desert located  
190 in the middle reaches of the HRB (Fig. 2a). The superstation includes a multiscale  
191 observation system for energy, water vapor and carbon fluxes (lysimeter-EC system-  
192 scintillometer for meter-hundred-kilometer observation scale) and soil moisture

193 measurements (*in situ* soil moisture profile-cosmic ray probe-soil moisture wireless  
194 sensor network for meter-hundred-kilometer observation scale), and it includes a  
195 hydrometeorological gradient observation system to monitor the profile (7 layers) of  
196 wind speed/direction, air temperature/humidity and carbon dioxide and water vapor  
197 concentration, one layer four-component radiation, air pressure, precipitation, and  
198 infrared temperature (2 repetitions), 9/8 layers' soil temperature/moisture profile, soil  
199 heat flux (3 plates with two buried under the bare soil between two corn plants and one  
200 buried under the corn plants), etc. The EC and hydrometeorological gradient  
201 observation system were installed on a 40 m tower. Optical and microwave  
202 scintillometers were installed on both sides of the 40 m tower apart from 1854 m. There  
203 were also observations of vegetation parameters in the 40 m tower, including a visible  
204 and near infrared phenological camera to monitor the vegetation index and crop growth  
205 curve, two photosynthetically active radiation (PAR) sensors to monitor PAR, a  
206 vegetation chlorophyll fluorescence observation system to monitor sun-induced  
207 chlorophyll fluorescence (SIF), and an LAI wireless sensor network (28 nodes) to  
208 monitor multipoint LAI in the source area of the scintillometer (Fig. 2b, Fig. 4a).

209 The ordinary stations are comprised of an EC system, an automatic weather station  
210 (AWS) and a visible and near infrared phenological camera. The observation elements  
211 of the AWS include two layers' air temperature/humidity and wind speed/direction, one  
212 layer's four-component radiation, air pressure, and infrared temperature (2 repetitions),  
213 two layers' precipitation, 8/7 layers' soil temperature/moisture, soil heat flux (3 plates),  
214 etc. (Fig. 2c).

215 The sonic anemometers of the ECs were installed at a height of approximately 3-7 m  
 216 above the canopy to capture the sensible heat, latent heat, carbon dioxide and methane  
 217 (in wetland) fluxes, etc. The sonic anemometers of all the ECs were aimed toward the  
 218 north. Soil parameters, such as soil texture, porosity, bulk density, saturated hydraulic  
 219 conductivity, and soil organic matter content, etc. were investigated at each station in  
 220 2012 and 2020. Detailed information can be found in Table 2.



221  
 222 Fig. 2. Sketch map of the artificial oasis and desert area in the middle reaches (a:  
 223 artificial oasis and desert area (from © Google Earth); b: Daman superstation; c:  
 224 Huazhaizi ordinary station)

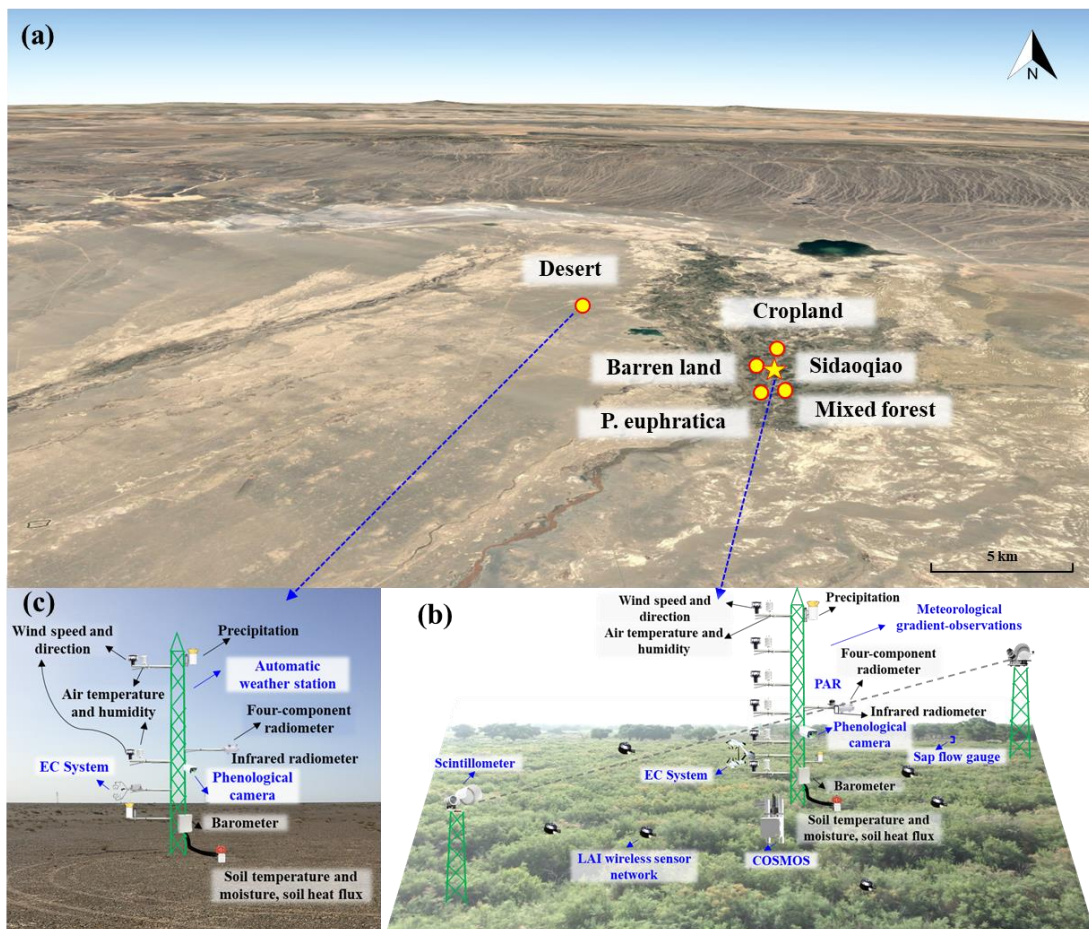
### 225 **2.2.2 Natural oasis and desert areas in the lower reaches**

226 The Ejin Banner oasis is located in the lower reaches of the HRB and belongs to  
227 Inner Mongolia and part of Jiuquan city of Gansu Province, which is surrounded by  
228 widespread desert. The main underlying surfaces were Reaumuria and terminal lake in  
229 desert, riparian forest, cropland, barren land and residential area in the oasis in the lower  
230 reaches. There were six stations (one superstation and five ordinary stations) in the  
231 lower reaches, which are located in these land covers, including *Populus euphratica*,  
232 *Tamarix chinensis*, cropland, barren land, and desert.

233 In the oasis-desert area of the lower reaches, there is one superstation and four  
234 ordinary stations in the oasis and one ordinary station in the desert (Fig. 3a). The  
235 superstations include a multiscale observation system for energy, water vapor and  
236 carbon fluxes (sap flow gauge-EC-large aperture scintillometer for meter-hundred-  
237 kilometer observation scale) and soil moisture measurements (*in situ* soil moisture  
238 profile and cosmic ray probe for meter and hundred meter observation scale), a  
239 hydrometeorological gradient observation system to monitor the profile (6 layers) of  
240 wind speed/direction, air temperature/humidity, one layer four-component radiation, air  
241 pressure, and infrared temperature (2 repetitions), two layers of precipitation, 10/9  
242 layers soil temperature/moisture profile, soil heat flux (with two buried under the bare  
243 soil and one buried under the *Tamarix* plants), etc. The EC and hydrometeorological  
244 gradient observation system were installed on a 28 m tower. Two groups of large  
245 aperture scintillometers were installed on both sides of the 28 m tower apart from 2350  
246 m. The vegetation parameter observations included PAR and the phenological camera

247 to monitor the vegetation index and crop growth curve installed in the 28 m tower and  
 248 LAI wireless sensor network (11 nodes in the source area of the scintillometer) (Fig. 3b,  
 249 Fig. 4b). The ordinary stations are comprised of an EC system, an AWS and a visible  
 250 and near infrared phenological camera. (Fig. 3c).

251 Additionally, thermal infrared radiometers and imagers were installed at the Mixed  
 252 Forest and Sidaoqiao stations to measure different component temperatures, i.e., the  
 253 brightness temperature of different land cover types under different illumination  
 254 conditions (Li et al., 2019). The soil parameters and groundwater table were observed  
 255 around the stations. Detailed information can be found in Table 2.



256  
 257 Fig. 3 Sketch map of the natural oasis and desert areas in the lower reaches (a: natural  
 258 oasis and desert area (from © Google Earth); b: Sidaoqiao superstation; c: desert

259 ordinary station)

260 Table 2 Observation variables and sensor configurations of surface flux,  
 261 hydrometeorology, vegetation and soil parameters

Observations	Sensor	Manufactory	Height/depth (m)	Sites
<i>Surface flux observations:</i>				
Sensible heat, latent heat, carbon dioxide, methane flux	CSAT3&Gill, Li7500&Li7500 A&Li7500DS& EC155&Li7700 CPEC310	Campbell and LiCor, USA	3~7 m above the canopy	All stations (methane observation only in wetland, closed path EC at Daman and Desert, stations)
Sensible and latent heat flux	BLS900 and MWSC-160	Scintec and RPG, Germany	23.92	Daman
	BLS900	Germany	25.5	Sidaoqiao
Sap flow	TDP 30	Rainroot, China	1.5	Mixed forest
<i>Hydrometeorological observations:</i>				
Pressure	PTB110	Vaisala, Finland	--	Bajitan, Shenshawo
	AV-410BP	Avalon, USA	--	Mixed Forest
	PTB210	Vaisala, Finland	--	Huazhaizi
	CS100	Campbell, USA	--	Daman, Wetland, Sidaoqiao, Desert
Precipitation	TE525MM	Texas Electronics, USA	--	Daman, Wetland, Huazhaizi, Bajitan, Shenshawo, Sidaoqiao, Desert
	52203	RM Young, USA	--	Mixed Forest
Wind speed/direction	Windsonic	Gill, UK	3,5,10,15,20,30,40 5,7,10,15,20,28	Daman, Sidaoqiao
			5,10	Wetland, Huazhaizi, Mixed forest
	010C/020C	Met One	5,10	Wetland, Desert
	03001	RM Young, USA	10 28	Bajitan, Shenshawo Populus euphratica
Air temperature/hu	HMP45D	Vaisala, Finland	28	Mixed Forest

midity	HC2S3	Vaisala, Finland	5,7,10,15,20,28	Sidaoqiao
	HMP45AC	Vaisala, Finland	5,10	Bajitan,Huazhaizi, Shenshawo,Wetland, Desert
			28	Populus euphratica
AV-14TH	Avalon	3,5,10,15,20,30,40	Daman	
Four- component radiation	CNR4	Kipp&Zonen, Netherland	10	Sidaoqiao
			22	Mixed Forest
	CNR1	Kipp&Zonen, Netherland	6	Wetland,Huazhaizi,Bajita n,Shenshawo,Desert,Barr en land, Cropland
			22	Populus euphratica
PSP&PIR	Eppley, USA	12	Daman	
Infrared temperature	SI-111	Apogee, USA	12	Daman
			10	Sidaoqiao
			22	Populus euphratica, Mixed Forest
			6	Wetland,Huazhaizi,Bajita n,Shenshawo,Desert,Barr en land, Cropland
Soil temperature profile	109ss-L	Campbell, USA	0,-0.02,-0.04,-0.1,- 0.2,-0.4,-0.8,-1.2,-1.6,- 2.0	Sidaoqiao, Desert Wetland
			0, -0.02,-0.04,-0.1,- 0.2,-0.4,-0.6,-0.8,-1.2,- 1.6	Daman
			0, -0.02,-0.04,-0.1,- 0.2,-0.4,-0.6,-1.0	Bajitan, Huazhaizi
			0, -0.02,-0.04,-0.1,- 0.2,-0.4	Wetland
	AV-10T	Avalon, USA	0,-0.02,-0.04,-0.1,- 0.2,-0.4,-0.6,-1.0,-1.6,- 2.0,-2.4	Mixed forest
			0, -0.02,-0.04,-0.1,- 0.2,-0.4,-0.6,-1.0	Shenshawo
			0, -0.02,-0.04	Barren land, Cropland, Populus euphratica
109	Campbell, USA	0, -0.02,-0.04		



Soil moisture profile	ECH <sub>2</sub> O-5	Decagon Devices, USA	-0.02,-0.04,-0.1,-0.2,-0.4,-0.6,-1.0	Bajitan
	CS616	Campbell, USA	-0.02,-0.04,-0.1,-0.2,-0.4,-0.6,-0.8,-1.2,-1.6	Shenshawo, Desert
	ML2X	Delta-T, UK	-0.02,-0.04,-0.1,-0.2,-0.4,-0.8,-1.2,-1.6,-2.0	Daman
			-0.02,-0.04,-0.1,-0.2,-0.4,-0.6,-1.0,-1.6,-2.0,-2.4	Sidaoqiao
			-0.02, -0.04	Mixed Forest
	ML3	Delta-T, UK	-0.02,-0.04,-0.1,-0.2,-0.4,-0.6,-1.0	Barren land, Populus euphratica, Cropland
Soil heat flux	HFP01	Hukseflux, Netherland	-0.06	Desert, Huazhaizi
	HFT3	Campbell, USA	-0.06	Wetland,Huazhaizi, Bajitan,Shenshawo,Desert,Barren land, Cropland
	HFP01SC	Hukseflux, Netherland	-0.06	Bajitan, Populus euphratica, Mixed forest
Averaged temperature	TCAV	Campbell, USA	-0.02, -0.04	Daman, Sidaoqiao
CO <sub>2</sub> /H <sub>2</sub> O profile	AP200	Campbell, USA	3,5,10,15,20,30,40	Daman
Groundwater Table	U20	Onset, USA	-2~-3m	Sidaoqiao, Mixed forest, Populus euphratica, Cropland, Desert
<i>Vegetation parameter observations:</i>				
Vegetation phenology	Phenological camera	XST-PhotoNet, China	above the canopy	All sites
LAI	XST-LAINet	Beijing StarViewer Science and Technology Ltd., China	Below the canopy	28 nodes around Daman, 6 nodes around Sidaoqiao, 5 nodes around Mixed forest
photosynthetically active radiation	PQS-1	Kipp&Zonen, Netherland	0.5, 12	Daman
			10	Sidaoqiao
			22	Mixed forest, Populus euphratica
			6	Wetland, Cropland

---

		Beijing		
Sun-induced		Bergsun		
chlorophyll	AutoSIF-1	Spectral	34	Daman
fluorescence		Technology		
		Co. Ltd, China		

---

*Soil parameters: soil sampling and laboratory testing in 2012 and 2020*

---

262

263 **3. Data processing and quality control**

264 The data processing and quality control procedure can be divided into data collection,  
 265 data processing and data archiving and sharing (Fig. 4).

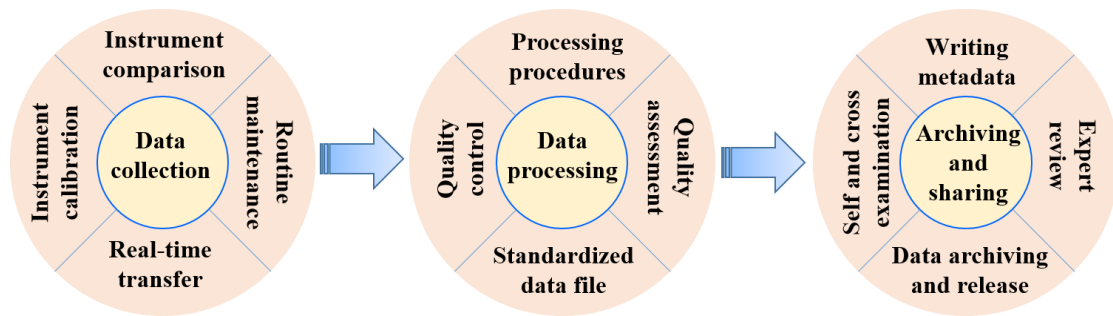
266 In the data collection step, the comparison and calibration of instruments are  
 267 prerequisites to ensure the quality of the observation data. The instrument comparison  
 268 experiments were specifically arranged under the Gobi Desert in 2012 in the middle  
 269 reaches (Xu et al., 2013) and shrub in 2013 in the lower reaches (Li et al., 2018) to  
 270 ensure the consistency and comparability of the instruments. In addition, the  
 271 instruments with multiple layers were compared at the same height before installation,  
 272 the soil moisture probes were also compared under dry and wet conditions, and the  
 273 multitype rain gauges were compared in the same field. The infrared gas analyzer of all  
 274 the EC systems was calibrated at the beginning and end of the vegetation-growing  
 275 season every year. To ensure the data quality, a routine maintenance procedure is  
 276 formulated and strictly followed, including daily (checking the real-time data through  
 277 remote monitoring and data management system for field observatory network v1.0),  
 278 10 days (checking the time series plot providing by the system), monthly (routine  
 279 inspection in every station), and annually (data processing and release) (Liu et al., 2018).  
 280 The Heihe watershed internet of things observation system was developed to complete

281 the above maintenance procedure, which included remote receiving and storing the filed  
282 data, browsing and processing real-time data, monitoring the instrument status and early  
283 warning the abnormal conditions, etc.

284 During the data processing step, a processing scheme was formulated for each type  
285 of instrument. For the EC system, the data were processed from the raw 10 Hz turbulent  
286 data, including spike detection, sonic temperature correction, coordinate rotation,  
287 frequency response correction, and WPL (Webb-Pearman-Leuning) correction. (Liu et  
288 al., 2016; Wu et al., 2023). Additionally, the 30-min flux data series were identified as  
289 quality flags according to the stationarity test and integral turbulence characteristics test.  
290 A final quality flag (1~9) was assigned to each specific turbulent flux value, indicating  
291 good quality (1~3), suitability for general use (4~6), poor but better than gap filling data  
292 (7~8), and discarded data (9). The unclosed energy balance of EC system is a universal  
293 problem. There was approximately an average of 17% energy imbalance in our study  
294 area (Xu et al., 2017; Zhou et al., 2018), which was reasonable compared with previous  
295 results (Stoy et al., 2013). The Bowen-ratio correction method is recommended to close  
296 the energy balance (Twine et al., 2000; Xu et al., 2020). The data processing steps from  
297 scintillometer measurements to surface fluxes are as follows: raw data to light intensity  
298 variance, light intensity variance to the structure parameter of the refractive index of air  
299 ( $C_n^2$ ),  $C_n^2$  to meteorological data, and finally obtaining surface fluxes combining the  
300 meteorological data. Four steps are taken to ensure the quality of scintillometer data  
301 (Liu et al. 2011; Zheng et al., 2023): (i) excluding data for  $C_n^2$  beyond the saturation  
302 criterion; (ii) excluding data obtained during periods of precipitation; (iii) excluding

303 data when the demodulated signal is small; and (iv) excluding data when the sensor is  
304 malfunctioning. The steps of the meteorological gradient observation system and AWS  
305 data processing and quality control were twofold: (1) all the AWS data were averaged  
306 over an interval of 10 min for a total of 144 records per day. The missing data were  
307 denoted by -6999; (2) the unphysical data were rejected, and the gaps were denoted by  
308 -6999. The surface soil heat flux was calculated using the ‘PlateCal’ approach  
309 (Liebethal et al., 2005), and the final surface soil heat flux was the weighted vegetation  
310 fraction combined with the soil temperature and moisture measured above the heat  
311 plates. There are approximately 10–20% missing or rejected values of EC or  
312 scintillometer data. The look-up table (LUT) method is recommended to fill the gaps  
313 when data were missing (Xu et al., 2020). The maximum missing values of AWS data  
314 were no more than 10%, and linear interpolation method is recommended to fill the  
315 missing values. The vegetation growth curve and vegetation index can be obtained from  
316 visible and near infrared bands measured by phenological cameras. The key  
317 phenological parameters are determined according to growth curve fitting, such as the  
318 growth season start date, peak, and growth season end. The leaf area index (LAI) data  
319 were obtained from the LAINet sensor, which can continuously measure the multipoint  
320 total solar radiation above the canopy and the transmitted radiation below the canopy,  
321 and the LAI was calculated based on multiangle transmittance data (Qu et al., 2014).  
322 Seven days moving averaged method is recommend to eliminate noise from the daily  
323 LAI observations (Qu et al., 2014). Then, all the data are processed into a standardized  
324 file for sharing.

325 During the archiving and sharing step, the metadata were written for each data point,  
 326 including the site description, processing step, header description, and other notes. (Li  
 327 et al., 2017a). Before data are released, self-examination, crosschecks and expert review  
 328 are required to ensure data quality. Finally, the data were archived and shared online.



329

330 Fig. 4 Flowchart of data processing and quality control

#### 331 4. Data description

##### 332 4.1 Energy, water vapor and carbon fluxes data

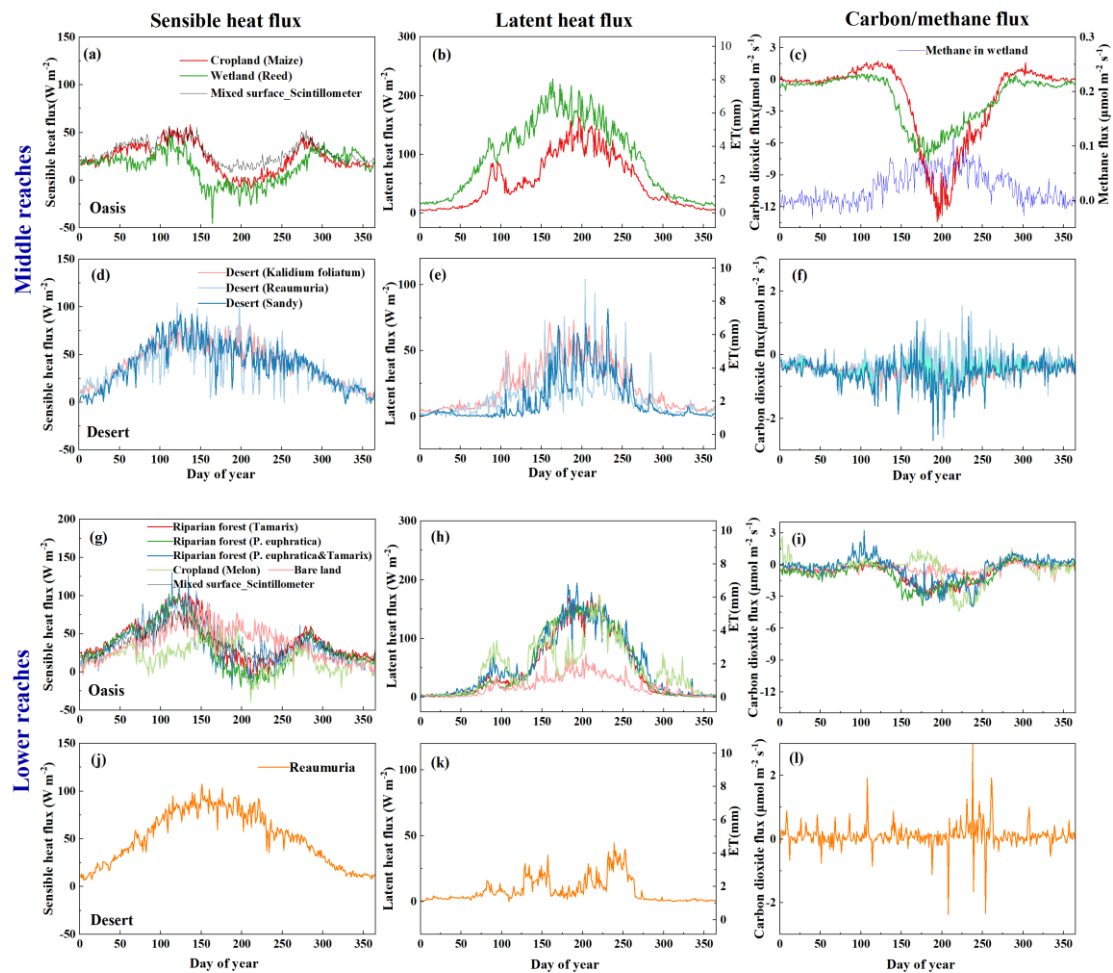
333 The EC systems were used to measure surface flux at all sites, namely, 5 stations (2  
 334 in oasis, 3 in desert) in the middle reaches and 6 stations (5 in oasis, 1 in desert) in the  
 335 lower reaches. The turbulent flux data were recorded by the open path or closed path  
 336 EC systems and processed carefully. In addition to the surface flux of sensible, latent  
 337 and carbon dioxide, the methane flux was also observed at the wetland site in the middle  
 338 reaches (Table 2). The multiyear seasonal variations in sensible heat, latent heat, carbon  
 339 dioxide and methane fluxes are shown in Figure 5. Generally, the latent heat fluxes in  
 340 oases are obviously higher than those in deserts, especially in the lower reaches. The  
 341 latent heat fluxes exhibited a single peak during one year, with a peak value of  
 342 approximately  $200 \text{ W m}^{-2}$  in the oasis area; however, they significantly fluctuated due  
 343 to irrigation (normally 4 times in cropland of the midstream region, 2 times in riparian  
 344 forest and melon of the downstream region) or precipitation. In the middle reaches, the  
 345 latent heat flux in the wetland showed the largest values, which were more than  $200 \text{ W}$

346  $\text{m}^{-2}$  in the crop growing season, and it also presented relatively large values in the  
347 midstream piedmont desert region with dense *Kalidium foliatum* cover (peak value  
348 greater than  $50 \text{ W m}^{-2}$ ). In the lower reaches, the latent heat flux showed consistent  
349 variations in the riparian forest with a peak value of approximately  $150 \text{ W m}^{-2}$  during  
350 the crop growing season; however, it showed large fluctuations in the melon surface  
351 during growth due to frequent irrigation (approximately 7~8 times), and the bare land  
352 in the oasis and desert had a small latent heat flux.

353 The seasonal variations in sensible heat flux were totally different in the oasis and  
354 desert systems. The sensible heat flux showed two peaks in the oasis in both the middle  
355 and lower reaches except for the bare land, namely, reaching maximum values at the  
356 end of April and September, and it showed minimum values in mid-August ( $-25 \text{ W m}^{-2}$ ),  
357 corresponding to large values of latent heat flux in the oasis that were even greater  
358 than net radiation. This phenomenon was also found by previous researchers (Liu et al.,  
359 2011) and was called the ‘oasis effect’. In the desert area, the sensible heat flux appeared  
360 as a single peak in spring and decreased gradually since then. The variation in sensible  
361 heat flux in bare land of the natural oasis in the lower reaches is similar to that in the  
362 desert area.

363 In the oasis, the carbon dioxide ( $\text{CO}_2$ ) flux showed obvious ‘U’ variations, especially  
364 in the middle reaches. The crop absorbed carbon dioxide (carbon sink) in the crop-  
365 growing season, and a negative value of approximately  $-14 \mu\text{mol m}^{-2} \text{ s}^{-1}$  was observed  
366 in the maize surfaces. The magnitude of the methane ( $\text{CH}_4$ ) flux was lower than the  
367  $\text{CO}_2$  flux and was in the range of approximately  $0\sim 0.1 \mu\text{mol m}^{-2} \text{ s}^{-1}$  in the wetland. The  
368  $\text{CH}_4$  flux in the non-growing season was the lowest and increased rapidly in April.  
369 Although the magnitude of the  $\text{CH}_4$  flux was lower than the  $\text{CO}_2$  flux, the contribution

370 of methane emissions to global warming was as important as CO<sub>2</sub> contributions on a  
 371 long time scale (Hommeltenberg et al., 2014; Zhang et al., 2016b), especially focusing  
 372 on CH<sub>4</sub> flux measurements in wetlands (Zhang et al., 2022). The variations in CO<sub>2</sub> flux  
 373 in the riparian forest were relatively small, with values of approximately -0.4 μmol m<sup>-2</sup>  
 374 s<sup>-1</sup> in the plant growing season. There was little carbon sequestration in the desert area  
 375 due to little or sparse vegetation, and the CO<sub>2</sub> flux in the desert area was very small,  
 376 fluctuating around zero during the years.



377  
 378 Fig. 5 The multiyear seasonal variations in sensible, latent heat, carbon dioxide and  
 379 methane fluxes in the oasis-desert area (sensible heat flux–left, latent sensible heat flux–  
 380 middle, carbon dioxide and methane flux–right, 2012-2021)

## 381 **4.2 Hydrometeorological data**

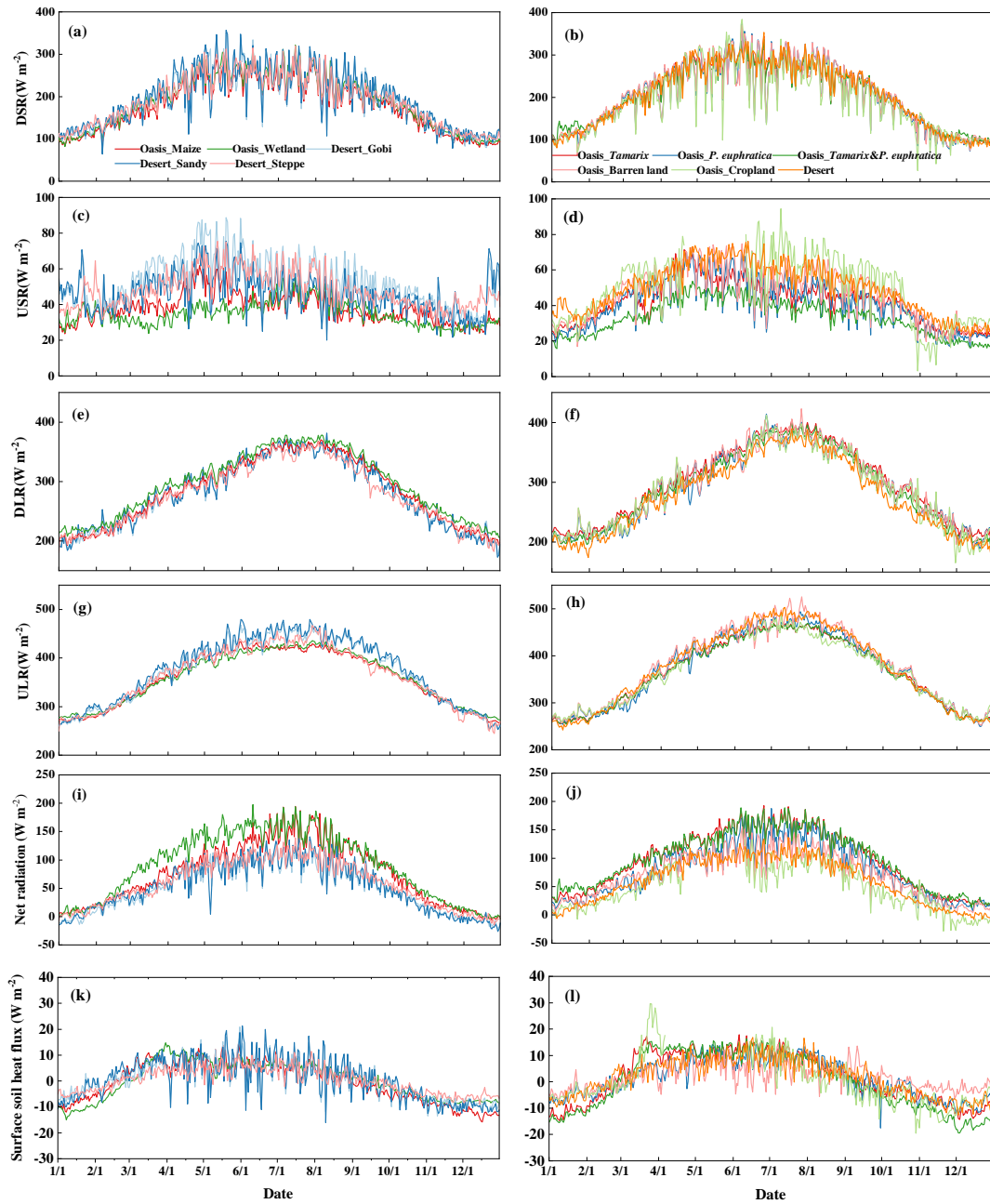
382 The hydrometeorological data were obtained from 13 AWSs, with six in the middle  
383 reaches (Fig. 2) and seven in the lower reaches (Fig. 3) of the HRB. All the AWSs  
384 recorded four-component radiations (short/long wave upward and downward radiation),  
385 soil heat flux, surface and soil temperature profiles, air temperature and humidity, wind  
386 speed and direction, air pressure, precipitation, soil moisture profiles, infrared  
387 temperature, and groundwater table in the lower reaches. (Table 2). All sensors were  
388 calibrated and intercompared before being mounted. The sampling frequencies,  
389 reference heights and directions of these sensors at all stations were identical to  
390 maintain consistency.

### 391 **4.2.1 Radiation, soil heat flux, surface and soil temperature profile**

392 It is important to understand the variations in radiation and surface soil heat flux in  
393 oasis and desert areas, which are the surface available energy. Figure 6 shows the four  
394 radiation components and soil heat flux in oasis and desert areas in the middle and lower  
395 reaches in the HRB, and all the variables exhibited obvious seasonal variations with an  
396 inverted 'U' shape. The incoming shortwave radiation was consistent with each other  
397 in oasis and desert because of the short distance among the sites. Due to the higher  
398 albedo in the desert, the upward shortwave radiation in the desert was larger than that  
399 in the oasis (approximately larger than 30%). The incoming longwave radiation  
400 originates from the atmosphere (in particular CO<sub>2</sub> and water vapor) and thermal  
401 radiation of clouds in the lower atmosphere. The oasis presents relatively large water  
402 vapor and cloudiness; thus, the incoming longwave radiation for the oasis was greater



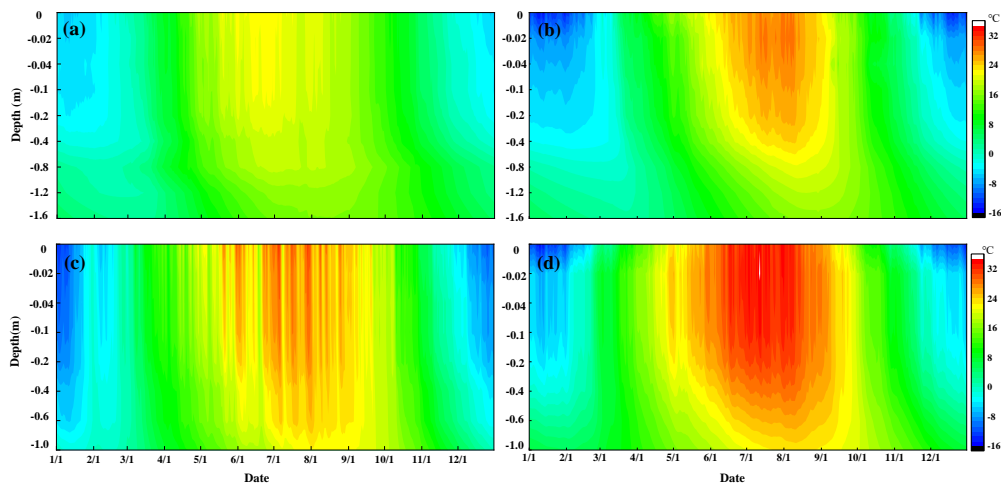
403 than that for the desert (approximately 2%). It is to be expected that under dry  
404 conditions during the daytime, the surface temperature of the desert will be significantly  
405 greater than that of the well-watered oasis site. Consequently, the upward longwave  
406 radiation in the desert was larger than that in the oasis (approximately 8%). The net  
407 radiation, driving the turbulent fluxes of sensible heat and latent heat at the earth surface  
408 and heating soil, was greater in the artificial oasis and the natural oasis than in the desert  
409 at approximately  $50 \text{ W m}^{-2}$ . The daily mean surface soil heat fluxes varied similarly in  
410 oasis and desert areas with relatively low values in the range of  $-20$  to  $20 \text{ W m}^{-2}$ .



411  
 412 Fig. 6 Seasonal variations in multiyear average radiation components in the oasis-desert  
 413 system (middle reaches: a, c, e, g, i, k; lower reaches: b, d, f, h, j, l; 2012-2021 daily  
 414 averaged DSR: downward shortwave radiation; USR: upward shortwave radiation;  
 415 DLR: downward longwave radiation; ULR: upward longwave radiation)

416 The soil temperature exhibited a signal peak around the year in the range of -  
 417 15°C~34°C, and it decreased with increasing soil depth during the plant growing season;  
 418 however, it exhibited an increasing trend in the winter. The shallow soil began to thaw

419 at the beginning of spring (march) and to freeze in autumn (November). The soil  
 420 temperature changed little with depth when it exceeded 0.8 m and 1 m in the oasis and  
 421 desert, respectively. The soil temperature in the desert was significantly higher by  
 422 approximately 10 °C during the plant growing season than that in the oasis in both the  
 423 middle and lower reaches. Additionally, the soil temperature in the artificial oasis-desert  
 424 area (middle reaches) was approximately 5 °C lower during the plant growing season  
 425 than that in the natural oasis-desert area (lower reaches) (Fig. 7).



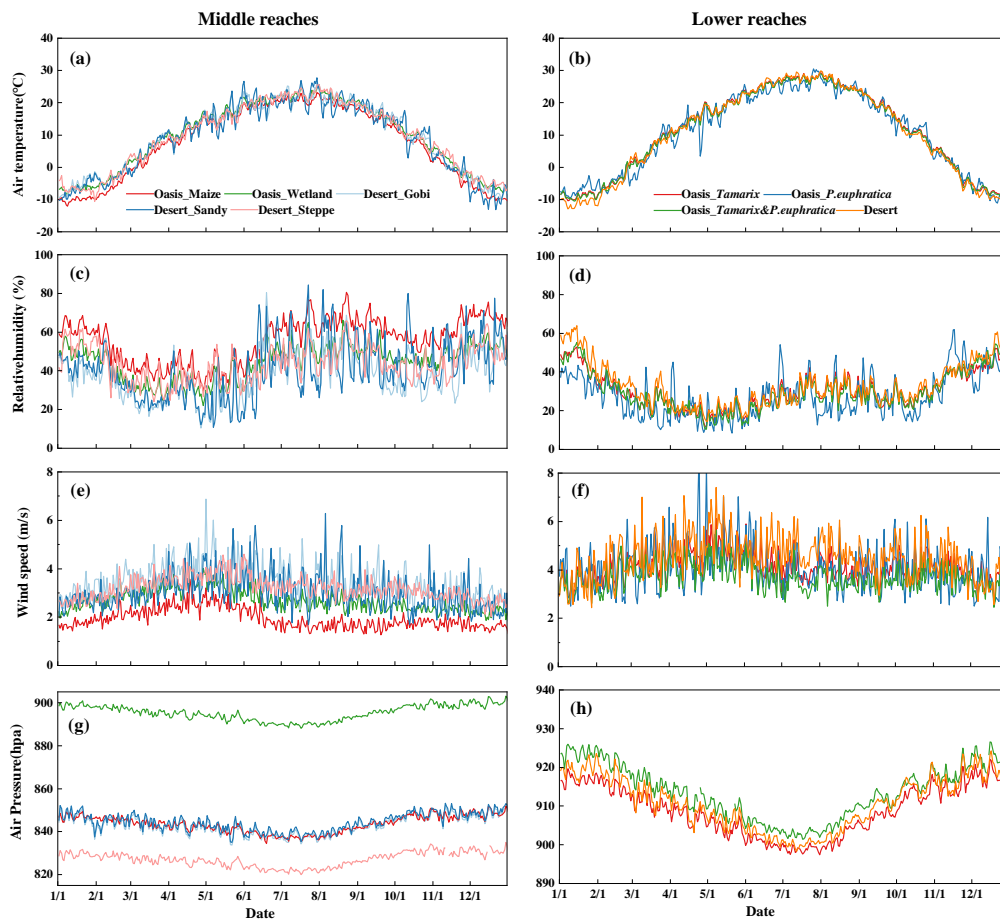
426  
 427 Fig. 7. Seasonal variations in surface and soil temperature profiles in oasis and desert  
 428 areas (2012-2021) (a: oasis in middle reaches–maize; b: oasis in lower reaches–*Tamarix*;  
 429 c: desert in middle reaches–*Reaumuria*; d: desert in lower reaches–*Reaumuria*)

#### 430 4.2.2 Air temperature/humidity, wind speed/direction, air pressure

431 To show micrometeorological characteristics clearly, the comparison of daily average  
 432 air temperature and relative humidity (5 m except the *P. euphratica* surface with a height  
 433 of 28 m), wind speed (10 m) and air pressure in desert and oasis are plotted in Figure 8.  
 434 The seasonal variation in air temperature in the oasis and desert was similar; however,  
 435 the air temperature in the desert was generally higher than that in the oasis by

436 approximately 0.6 °C on average annually (approximately 0.4 °C in the plant growing  
437 season). Instead, the relative humidity in the desert was lower than that in the artificial  
438 oasis in the midstream region (approximately 9% and 10% in the annual and plant  
439 growing seasons, respectively). The relative humidity in natural oasis and desert areas  
440 are similar due to the extreme arid regions with rare precipitation, little irrigation  
441 amount and small natural oasis area. Generally, the desert surface has the characteristics  
442 of high temperature and lower humidity, and the oasis is a cold and wet island. In the  
443 middle and lower reaches of the oasis and desert areas, the wind speed in the desert was  
444 obviously larger than that in the oasis because of the wind shield effect in the oasis  
445 (middle reaches: 1~3 m/s in the oasis, 2~6 m/s in the desert; lower reaches: 3~6 m/s in  
446 the oasis, 3~7 m/s in the desert), and the wind speed decreased significantly when  
447 passing by the windbreaks, buildings and crops, especially in the artificial oasis in the  
448 middle reaches. The lower wind speed in oases is helpful to plant growth, people's  
449 survival environment and the maintenance of oasis and desert ecosystems (Wang and  
450 Cheng, 1999). While the seasonal variation in wind speed between desert and oasis was  
451 similar, this indicated that they were controlled by the same synoptic system. The wind  
452 speed in the natural oasis in the lower reaches was higher than that in the artificial oasis  
453 in the middle reaches. The maximum wind speeds were observed in April in the  
454 artificial and natural oases, respectively, while the minimum values were observed in  
455 July. The air pressure decreased with decreasing elevation, e.g., the air pressure in the  
456 middle reaches with relative high elevation was lower than that in the lower reaches, as  
457 well as the discrete distribution of stations in the middle reaches with different

458 elevations (Fig. 10g and h, Table 1).

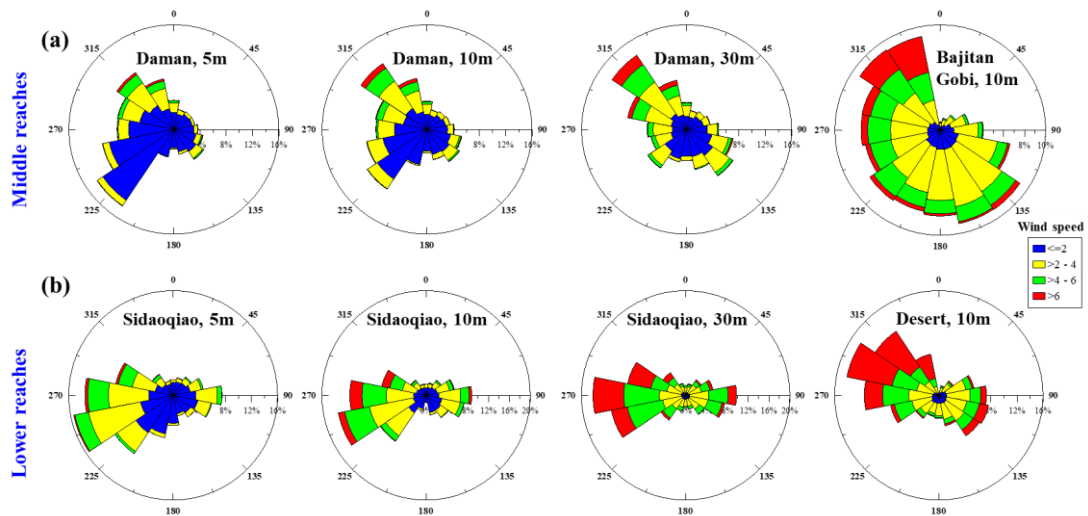


459

460 Fig. 8 Micrometeorological comparison between the oasis and desert (a, b: air  
461 temperature; c, d: relative humidity; e, f: wind speed; g, h: air pressure, 2012-2021)

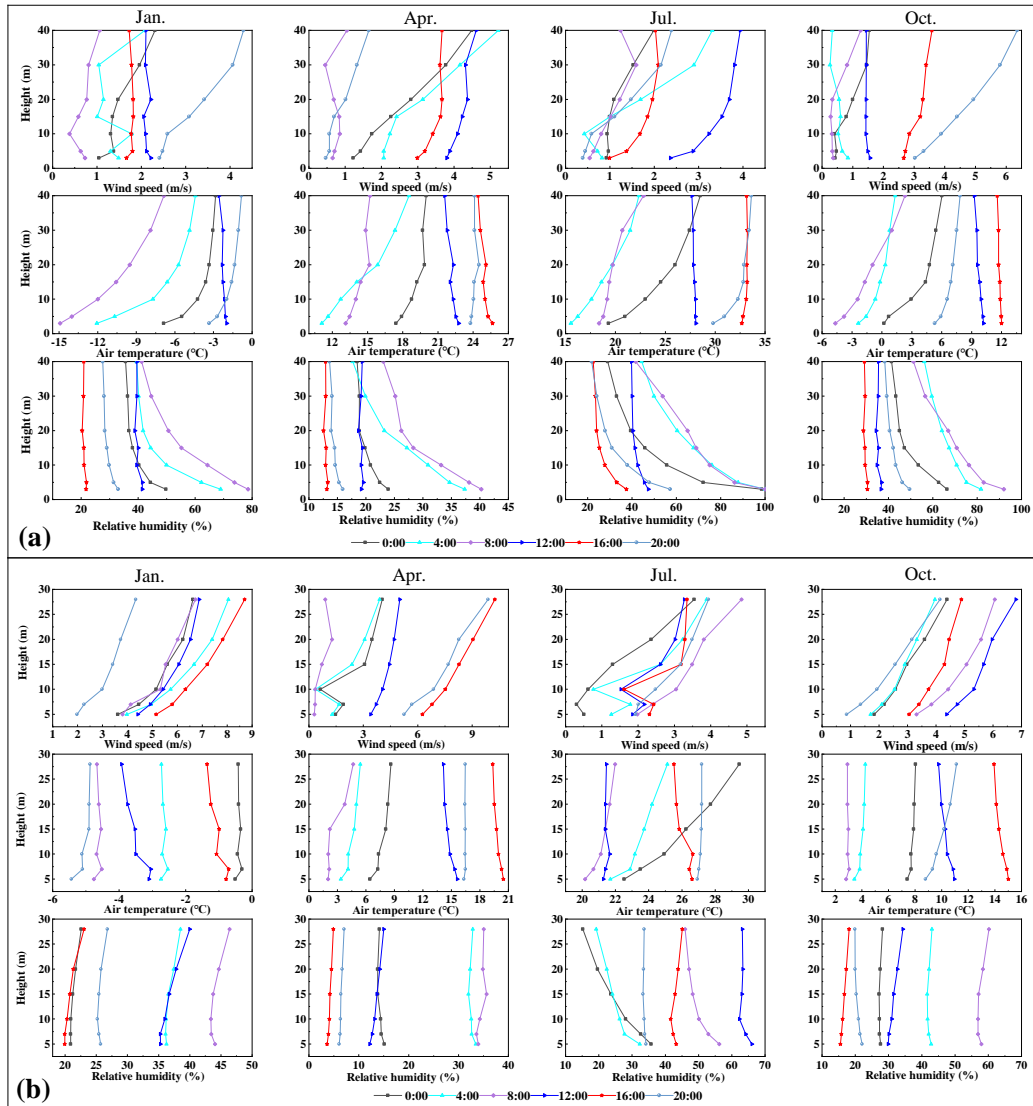
462 Windbreaks, buildings, crops or riparian forests drag on the wind flow inside the oasis,  
463 and the wind direction is different in the oasis and desert. In the middle reaches, the  
464 dominant wind directions in the desert are the northwest wind and southeast wind  
465 directions, while they are northwest and southwest (10 m) in the oasis cropland;  
466 however, with the increase in observation height, the influence of surface roughness on  
467 wind speed/direction decreased, and the southwest wind gradually decreased, while the  
468 northwest wind and southeast wind gradually increased, which is similar to the wind in  
469 the desert area around the oasis (~30 m height). In the lower reaches, the wind direction

470 was similar in the oasis and desert areas, with prevailing wind directions of west and  
 471 east (Fig. 9).



472  
 473 Fig. 9 Wind speed/direction in the oasis and desert area (2012-2021) (a: artificial oasis-  
 474 desert area in middle reaches; b: natural oasis-desert area in lower reaches; legend is  
 475 wind speed)

476 There are six/seven layer gradient observations of wind, air temperature and  
 477 humidity in superstations in artificial and natural oases. Data on typical days during  
 478 January, April, July and October in 2021 were selected, and the profiles of wind speed,  
 479 air temperature and humidity are plotted in Fig. 10. The wind speed generally increased  
 480 with the observation height, especially in the natural oasis. The air temperature showed  
 481 inversion at night during atmospheric stable stratification and changed little even below  
 482 10 m in the afternoon in July at both artificial and natural oases, which may be caused  
 483 by oasis-desert interactions. The relative humidity was low during the daytime and  
 484 maintained high values at night, decreasing with the observation height, especially  
 485 below 10 m.



486

487 Fig. 10 The profile of wind speed, air temperature and relative humidity in typical days  
 488 of January 14, April 14, July 14 and October 14 in 2021 (a: artificial oasis in middle  
 489 reaches; b: natural oasis in lower reaches)

490 **4.2.3 Precipitation, soil moisture and groundwater table**

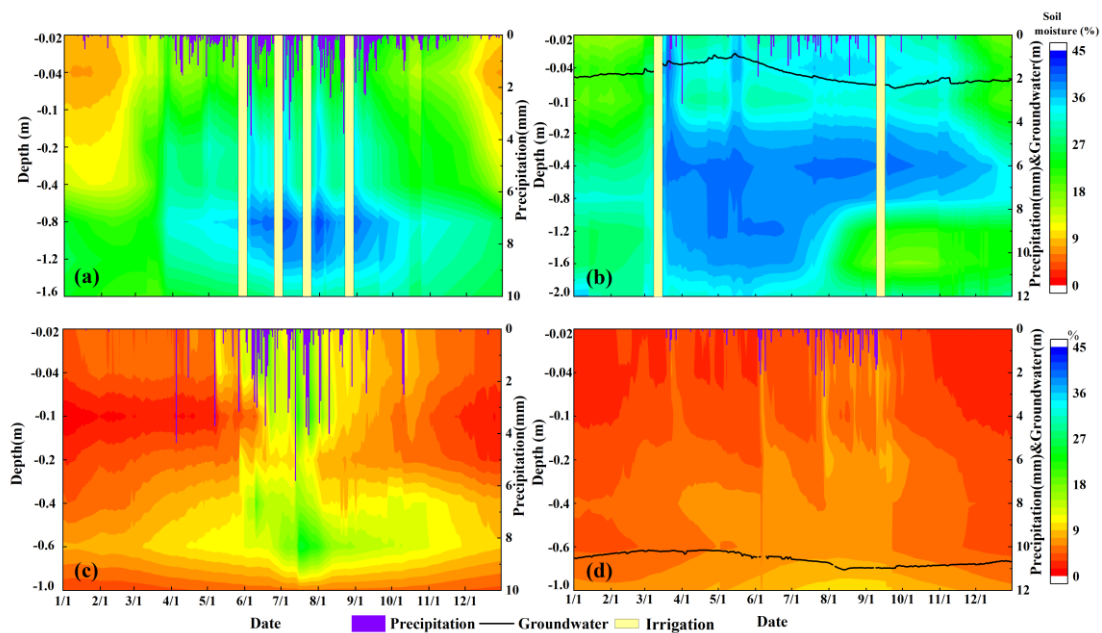
491 Figure 11 shows the variations in precipitation, soil moisture profiles and  
 492 groundwater table (lower reaches) in typical oasis and desert ecosystems. Precipitation  
 493 in the middle reaches was higher than that in the lower reaches, and it was higher in the  
 494 oasis than in the desert. The soil moisture in the oasis was significantly higher than that

495 in the desert, and it was especially small in the desert of the lower reaches. The soil  
496 moisture exhibited an increasing trend with increasing soil depth, especially in the oasis.  
497 The soil moisture was higher at depths of 0.8-1 m in the artificial oasis in the middle  
498 reaches and at depths of 0.4-0.8 m in the natural oasis in the lower reaches. Soil crust  
499 appeared in the lower reaches due to soil salinization, and it may prevent the loss of soil  
500 moisture. When a precipitation event occurred, the soil moisture in the desert increased  
501 accordingly; however, there were no clear variations in the oasis. There were usually  
502 four irrigation events in the artificial oasis in the middle reaches, and the soil moisture  
503 increased clearly accordingly, while some occasional peaks in soil moisture were due  
504 to relative heavy precipitation (Fig. 11a). In the lower reaches, two irrigation events  
505 (usually in March and September) generally occurred in riparian forests in natural oases.  
506 The shallow soil moisture showed large values in March when irrigation occurred and  
507 decreased in the plant growing season with a slight increase in September. Another  
508 phenomenon is that the precipitation in the artificial oasis was larger than that in the  
509 desert, although the sites were not far away from each other (e.g., 103.1 mm at the  
510 Daman superstation and 75.4 mm at the Gobi station). From the analysis, the soil  
511 moisture in the desert was strongly dependent on precipitation (Fig. 11c, d), while it  
512 maintained high values in the plant growth season relying on irrigation in the oasis.

513 In the lower reaches, five systems for groundwater table measurement have operated  
514 since June 2014 in the oasis, near the Sidaoqiao, Mixed Forest, *Populus euphratica*,  
515 Cropland, and Barren Land stations. The groundwater table was approximately 1–3 m  
516 under the ground, and the groundwater table level declined from a depth of



517 approximately 1 m to 3 m in the growing season to supply the riparian forest growth  
 518 (Fig. 11b). Additionally, one groundwater table measurement system was installed near  
 519 the desert station in 2018. The depth of the groundwater table level was approximately  
 520 10-11 m in the desert and showed no significant variation over the years (Fig. 11d).

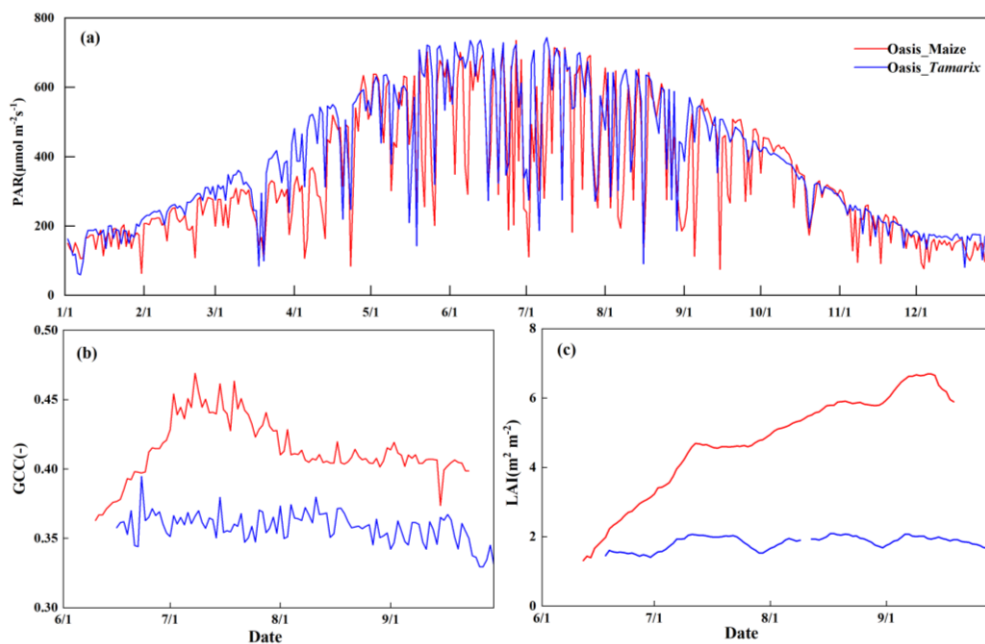


521  
 522 Fig. 11. Comparison of precipitation and soil moisture profile between desert and oasis  
 523 (2012-2021, a: oasis in the middle reaches (maize, Daman); b: oasis in the lower reaches  
 524 (*Tamarix*, Sidaoqiao); c: desert in middle reaches (Bajitan Gobi); d: desert in lower  
 525 reaches (desert))

### 526 4.3 Vegetation and soil parameters

527 The vegetation parameters include photosynthetically active radiation (PAR), leaf  
 528 area index (LAI), phenology, sun-induced chlorophyll fluorescence (SIF), etc. The PAR,  
 529 the amount of light available for photosynthesis, is observed at stations with vegetation  
 530 cover, and it can be used as the source of energy for photosynthesis by green plants.

531 The PAR observations showed similar seasonal variations in typical oasis ecosystems  
 532 in the middle and lower reaches, with a maximum daily PAR of approximately 750  
 533  $\mu\text{mol m}^{-2} \text{s}^{-1}$  (Fig. 14a). Vegetation parameters, such as LAI and phenology, were also  
 534 observed in the middle and lower reaches. LAI in the middle reaches (maize) increased  
 535 gradually with crop growth, and it was larger than that in the lower reaches (*Tamarix*),  
 536 which showed little change in this shrub surface (Fig. 14b). The phenological camera  
 537 was installed at each station except the desert to acquire the phenology. The greenness  
 538 index of the green chromatic coordinate (GCC) was derived to capture the key  
 539 phenological phase of the plant, such as the SOS (start of season), POP (position of  
 540 peak value), and EOS (end of season) (Fig. 14c).



541  
 542 Fig. 12. Variations in vegetation parameters in the middle and lower reaches of the oasis  
 543 (a, b, c are PAR, LAI and GCC in the artificial and natural oases, respectively, in 2018)

544 Soil samples were collected at each station in the middle and lower reaches in 2012  
 545 and 2020. These soil samples were analyzed in the laboratory, and parameters such as

546 soil texture, porosity, bulk density, saturated hydraulic conductivity, and soil organic  
 547 matter content were obtained. Some soil parameters at typical stations are shown in  
 548 Table 3. Silty soil is dominant in the oasis, and sand is dominant in the desert. The  
 549 porosity and bulk density showed no significant difference. The saturated hydraulic  
 550 conductivity and soil organic matter at the typical stations are also given in Table 3.

551 Table 3 Soil parameter measurements at typical stations in 2020

	Station	Soil texture	Soil properties
Middle reaches	Daman (Oasis)	Clay: 6% Silt: 69% Sand: 25%	Porosity: 47.1 %; Bulk density: 1.46 g/cm <sup>3</sup> ; Saturated hydraulic conductivity: 0.177 mm/min; Saturated water capacity: 64.10 %; PH: 8.48; NH <sub>4</sub> <sup>+</sup> -N: 0.83 mg/kg; NO <sub>3</sub> <sup>-</sup> -N: 15.90 mg/kg; Soil carbon content: 1.85 %; Soil organic carbon content: 0.72 %; Soil nitrogen content: 0.027%
	Huaizhaizi (Desert)	Clay: 1% Silt: 19% Sand: 80%	Porosity: 38.0 %; Bulk density: 1.49 g/cm <sup>3</sup> ; Saturated hydraulic conductivity: 4.93 mm/min; Saturated water capacity: 22.21 %; PH: 8.27; NH <sub>4</sub> <sup>+</sup> -N: 0.77 mg/kg; NO <sub>3</sub> <sup>-</sup> -N: 29.70 mg/kg; Soil carbon content: 1.83 %; Soil organic carbon content: 0.33 %; Soil nitrogen content: 0.026%
Lower reaches	Sidaoqiao (Oasis)	Clay: 21% Silt: 69% Sand: 10%	Porosity: 45.8 %; Bulk density: 1.47 g/cm <sup>3</sup> ; PH: 8.80; NH <sub>4</sub> <sup>+</sup> -N: 1.02 mg/kg; NO <sub>3</sub> <sup>-</sup> -N: 5.23 mg/kg; Soil carbon content: 2.02 %; Soil organic carbon content: 0.70 %; Soil nitrogen content: 0.070%
	Desert around terminal lake (Desert)	Clay: 9% Silt: 7% Sand: 84%	Porosity: 44.4 %; Bulk density: 1.49 g/cm <sup>3</sup> ; PH: 8.62; NH <sub>4</sub> <sup>+</sup> -N: 0.26 mg/kg; NO <sub>3</sub> <sup>-</sup> -N: 5.74 mg/kg; Soil carbon content: 1.42 %; Soil organic carbon content: 0.38 %; Soil nitrogen content: 0.039%

552 **5. Data availability**

553 The dataset of energy, water vapor and carbon exchange observations in oasis-desert  
 554 areas reported in this study, including energy, water vapor and carbon fluxes,  
 555 hydrometeorological data, and vegetation and soil parameters, are available and can be  
 556 downloaded freely at the National Tibetan Plateau Data Center  
 557 (<https://doi.org/10.11888/Terre.tpdc.300441>, Liu et al., 2023). A specific directory for  
 558 each observation station was designated with data classified into three categories,  
 559 namely, energy, water vapor and carbon fluxes, hydrometeorological data, and

560 vegetation and soil parameter data. Short descriptions were also provided for each  
561 dataset. The Beijing standard time was used in all the data files (UTC+8).

## 562 **6. Conclusions**

563 The typical land covers in the middle and lower reaches over the HRB are oases and  
564 deserts characterized by fragile environments. Oasisization and desertification are two  
565 opposing processes in arid and semiarid regions with scarce water resources. To combat  
566 desertification around oases and maintain the sustainable development of oases, a land  
567 surface process integrated observatory network was established in the oasis-desert area  
568 in the middle and lower reaches of the HRB. Eleven stations (7 in oasis, 4 in desert)  
569 have been established in these regions since 2012 to monitor the energy, water vapor  
570 and carbon exchange between land and atmosphere over oasis and desert areas, and a  
571 long-term and high-quality oasis and desert dataset of energy, water vapor and carbon  
572 fluxes and auxiliary parameters was produced. This study shows the achievements of  
573 11 stations over 10 continuous years of observations, including energy, water vapor and  
574 carbon fluxes, hydrometeorology, vegetation and soil parameter data. These data can  
575 be used in the analysis of the water-heat-carbon process and its influence mechanism  
576 (Wang et al., 2019; Xu et al., 2020; Bai et al., 2021; Wu et al., 2023), calibration and  
577 validation of remote sensing products (Ma et al., 2018; Song et al., 2018; Li et al., 2021;  
578 Zhang et al., 2022), and simulations of energy, water vapor and carbon exchange (Li et  
579 al., 2017b; Liu et al., 2020; He et al., 2022; Zhou et al., 2022). We confirm that the 10-  
580 year long-term dataset presented in this study is of high quality with few missing data  
581 and believe that the datasets will support ecological security and sustainable

582 development in oasis-desert areas. Most of the stations are ongoing observations, which  
583 can play a greater role in such ecologically fragile areas and provide a reference for  
584 other similar oasis-desert areas along the Silk Road.

#### 585 **Author contributions**

586 SL, ZX, TC and XL designed the framework of this work. SL and ZX performed the  
587 computations and data analysis and wrote the paper. ZR, YZ, and JT maintained the  
588 intensive experiment and downloaded the original measurements. TX, LS, JZ, ZZ, XY,  
589 RL and YM supervised the progress of this work, provided critical suggestions, and  
590 revised the paper.

#### 591 **Competing interests**

592 The authors declare that they have no conflict of interest.

#### 593 **Disclaimer**

594 Publisher's note: Copernicus Publications remains neutral with regard to jurisdictional  
595 claims in published maps and institutional affiliations.

#### 596 **Acknowledgement**

597 This work was supported by the Strategic Priority Research Program of the Chinese  
598 Academy of Sciences (Grant no. XDA20100101), the National Natural Science  
599 Foundation of China (42171461).

#### 600 **Financial support**

601 This work was supported by the Strategic Priority Research Program of the Chinese  
602 Academy of Sciences (Grant no. XDA20100101), the National Natural Science  
603 Foundation of China (42171461).

604 **Review statement**

605 This paper was edited by Zhen Yu and reviewed by two anonymous referees.

606 **References:**

607 Bai, Y., Liu, Y. L., Kueppers, L. M., Feng, X., Yu, K. L., Yang, X. F., Li, X. Y., and

608 Huang, J. P.: The coupled effect of soil and atmospheric constraints on stress-

609 responses of desert riparian species, *Agr. Forest Meteorol.*, 311, 108701,

610 <https://doi.org/10.1016/j.agrformet.2021.108701>, 2021.

611 Che, T., Dai, L.Y., Wang, J., Zhao, K., and Liu, Q: Estimation of snow depth and snow

612 water equivalent distribution using airborne microwave radiometry in the Binggou

613 Watershed, the upper reaches of the Heihe River basin, *Int. J. Appl. Earth Obs.*, 17,

614 23-32, <https://doi.org/10.1016/j.jag.2011.10.014>, 2012.

615 Che, T., Li, X., Liu, S.M., Li, H.Y., Xu, Z.W., Tan, J.L., Zhang, Y., Ren, Z.G., Xiao, L.,

616 Deng, J., Jin, R., Ma, M.G., Wang, J., and Yang, X.F.: Integrated hydrometeorological,

617 snow and frozen-ground observations in the alpine region of the Heihe River Basin,

618 China, *Earth Syst. Sci. Data*, 11, 1483–1499, 2019.

619 Cheng, G. D., Xiao, D. N., and Wang, G. X.: On the characteristics and building of

620 landscape ecology in arid area, *Adv. Geosci.*, 14 (1), 11–15, 1999. (in Chinese with

621 English abstract).

622 Cheng, G. D., Li, X., Zhao, W., Xu, Z., Feng, Q., Xiao, S. and Xiao, H.: Integrated study

623 of the water-ecosystem-economy in the Heihe River Basin, *Natl. Sci. Rev.*, 1(3), 413-

624 428, <https://doi.org/10.1093/nsr/nwu017>, 2014.

625 Chu, P. C., Lu, S., and Chen, Y.: A numerical modeling study on desert oasis self-

626 supporting mechanisms, *J. Hydrol.*, 312, 256-276,  
627 <https://doi.org/10.1016/j.jhydrol.2005.02.043>, 2005.

628 Crétaux, J. F., Calmant, S., Romanovski, V., Shabunin, A., Lyard, F., Bergé-Nguyen,  
629 M., Cazenave, A., Hernandez, F., and Perosanz, F.: An absolute calibration site for  
630 radar altimeters in the continental domain: Lake Issykkul in the central Asia, *J.*  
631 *Geodesy*, 83(8), 723-735, <http://doi.org/10.1007/s00190-008-0289-7>, 2009.

632 Dregne, H. E.: Global status of desertification, *Annals of Arid Zone*, 30, 179–185,  
633 <https://epubs.icar.org.in/index.php/AAZ/article/view/64733>, 1991.

634 Georgescu, M., Moustaoui, M., Mahalov, A., and Dudhia, J.: An alternative explanation  
635 of the semiarid urban area “oasis effect”, *J. Geophys. Res.-Atmos.*, 116, D24113,  
636 <https://doi.org/10.1029/2011JD016720>, 2011.

637 He, X. L., Liu, S. M., Xu, T. R., Yu, K. L., Gentile, P., Zhang, Z., Xu, Z. W., Jiao, D.  
638 D., and Wu, D. X.: Improving predictions of evapotranspiration by integrating multi-  
639 source observations and land surface model, *Agr. Water Manage.*, 272, 107827,  
640 <https://doi.org/10.1016/j.agwat.2022.107827>, 2022.

641 Hommeltenberg, J., Mauder, M., Drosler, M., Heidbach, K., Werle, P., and Schmid, H.  
642 P.: Ecosystem scale methane fluxes in a natural temperate bog-pine forest in  
643 southern Germany, *Agric. For. Meteorol.*, 198–199, 273–284,  
644 <https://doi.org/10.1016/j.agrformet.2014.08.017>, 2014.

645 Huang, J. P., Yu, H. P., Guan, X. D., Wang, G. Y., and Guo, R. X.: Accelerated dryland  
646 expansion under climate change, *Nature Clim. Change*, 6, 166-171,  
647 <https://doi.org/10.1038/nclimate2837>, 2016.

648 Liebenthal, C., Huwe, B., and Foken, T.: Sensitivity analysis for two ground heat flux  
649 calculation approaches, *Agric. For. Meteorol.*, 132(3–4), 253–262,  
650 <https://doi.org/10.1016/j.agrformet.2005.08.00>, 2005.

651 Li, M. S., Zhou, J., Peng, Z. X., Liu, S. M., Göttsche, F. M., Zhang, X. D., and Song, L.  
652 S.: Component radiative temperatures over sparsely vegetated surfaces and their  
653 potential for upscaling land surface temperature, *Agric. For. Meteorol.*, 276-277,  
654 107600, <https://doi.org/10.1016/j.agrformet.2019.05.031>, 2019.

655 Li, X., Li, X. W., Li, Z. Y., Ma, M. G., Wang, J., Xiao, Q., Liu, Q., Che, T., Chen, E. X.,  
656 Yan, G. J., Hu, Z. Y., Zhang, L. X., Chu, R. Z., Su, P. X., Liu, Q. H., Liu, S. M.,  
657 Wang, J. D., Niu, Z., Chen, Y., Jin, R., Wang, W. Z., Ran, Y. H., and Xin, X.:  
658 Watershed Allied Telemetry Experimental Research, *J. Geophys. Res.-Atmos.*,  
659 114, D22103, <https://doi.org/10.1029/2008JD011590>, 2009.

660 Li, X., Cheng, G. D., Liu, S. M., Xiao, Q., Ma, M. G., Jin, R., Che, T., Liu, Q. H., Wang,  
661 W. Z., Qi, Y., Wen, J. G., Li, H. Y., Zhu, G. F., Guo, J. W., Ran, Y. H., Wang, S. G.,  
662 Zhu, Z. L., Zhou, J., Hu, X. L., and Xu, Z. W.: Heihe Watershed Allied Telemetry  
663 Experimental Research (HiWATER): Scientific Objectives and Experimental  
664 Design, *B. Am. Meteorol. Soc.*, 94, 1145–1160, [https://doi.org/10.1175/BAMS-D-](https://doi.org/10.1175/BAMS-D-12-00154.1)  
665 12-00154.1, 2013.

666 Li, X., Yang, K., and Zhou, Y.: Progress in the study of oasis-desert interactions, *Agric.*  
667 *For. Meteorol.*, 230, 1-7, <https://doi.org/10.1016/j.agrformet.2016.08.022>, 2016.

668 Li, X., Liu, S. M., Xiao, Q., Ma, M. G., Jin, R., Che, T., Wang, W. Z., Hu, X. L., Xu, Z.  
669 W., Wen, J. G., and Wang, L. X.: A multiscale dataset for understanding complex



670 eco-hydrological processes in a heterogeneous oasis system, *Sci. Data*, 4, 170083,  
671 <https://doi.org/10.1038/sdata.2017.83>, 2017a.

672 Li, X., Zheng, Y., Sun, Z., Tian, Y., Zheng, C. M., Liu, J., Liu, S. M., and Xu, Z. W.: An  
673 integrated ecohydrological modeling approach to exploring the dynamic  
674 interaction between groundwater and phreatophytes, *Ecol. Model.*, 356, 127-140,  
675 <https://doi.org/10.1016/j.ecolmodel.2017.04.017>, 2017b.

676 Li, X., Liu, S. M., Li, H. X., Ma, Y. F., Wang, J. H., Zhang, Y., Xu, Z. W., Xu, T. R.,  
677 Song, L. S., Yang, X. F., Lu, Z., Wang, Z. Y., and Guo, Z. X.: Intercomparison of  
678 six upscaling evapotranspiration methods: from site to the satellite pixel, *J.*  
679 *Geophys. Res.-Atmos.*, 123, 6777-6803, <https://doi.org/10.1029/2018JD028422>,  
680 2018.

681 Li, X., Liu, S. M., Yang, X. F., Ma, Y. F., He, X. L., Xu, Z. W., Xu, T. R., Song, L. S.,  
682 Zhang, Y., Hu, X., Qu, Q., and Zhang, X. D.: Upscaling evapotranspiration from a  
683 single-site to satellite pixel scale, *Remote Sen.*, 13, 4072,  
684 <https://doi.org/10.3390/rs13204072>, 2021.

685 Liu, R., Sogachev, A., Yang, X. F., Liu, S. M., Xu, T. R., and Zhang, J. J.: Investigating  
686 microclimate effects in an oasis-desert interaction zone, *Agric. For. Meteorol.*, 290,  
687 107992, <https://doi.org/10.1016/j.agrformet.2020.107992>, 2020.

688 Liu, S. M., Xu, Z. W., Wang, W. Z., Bai, J., Jia, Z. Z., Zhu, M. J., and Wang, J. M.: A  
689 comparison of eddy-covariance and large aperture scintillometer measurements  
690 with respect to the energy balance closure problem. *Hydrol. Earth Syst. Sci.*, 15(4),  
691 1291-1306, <https://doi.org/10.5194/hess-15-1291-2011>, 2011.

692 Liu, S. M., Xu, Z. W., Song, L. S., Zhao, Q. Y., Ge, Y., Xu, T. R., Ma, Y. F., Zhu, Z. L.,  
693 Jia, Z. Z., and Zhang, F.: Upscaling evapotranspiration measurements from multi-  
694 site to the satellite pixel scale over heterogeneous land surfaces, *Agric. For.*  
695 *Meteorol.*, 230-231, 97-113, <https://doi.org/10.1016/j.agrformet.2016.04.008>,  
696 2016.

697 Liu, S. M., Li, X., Xu, Z. W., Che, T., Xiao, Q., Ma, M. G., Liu, Q. H., Jin, R., Guo, J.  
698 W., Wang, L. X., Wang, W. Z., Qi, Y., Li, H. Y., Xu, T. R., Ran, Y. H., Hu, X. L.,  
699 Shi, S. J., Zhu, Z. L., Tan, J. L., Zhang, Y., and Ren, Z.G.: The Heihe Integrated  
700 Observatory Network: A basin-scale land surface processes observatory in China,  
701 *Vadose Zone J.*, 17, 180072, <https://doi.org/10.2136/vzj2018.04.0072>, 2018.

702 Liu, S., Xu, Z., Che, T., Li, X., Xu, T., Ren, Z., Zhang, Y., Tan, J., Song, L., Zhou, J.,  
703 Zhu, Z., Yang, X., Liu, R., and Ma, Y.: Energy, water vapor and carbon exchange  
704 observations in oasis-desert areas of Heihe river basin (2012-2021), National  
705 Tibetan Plateau/Third Pole Environment Data Center,  
706 <https://doi.org/10.11888/Terre.tpd.300441>, 2023.

707 Ma, Y. F., Liu, S. M., Song, L. S., Xu, Z. W., Liu, Y. L., Xu, T. R., and Zhu, Z. L.:  
708 Estimation of daily evapotranspiration and irrigation water efficiency at a Landsat-  
709 like scale for an arid irrigation area using multi-source remote sensing data, *Remote*  
710 *sens. environ.*, 216, 715-734, <https://doi.org/10.1016/j.rse.2018.07.019>, 2018.

711 Mao, D., Wang, Z., Wu, B., Zeng, Y., Luo, L., and Zhang, B: Land degradation and  
712 restoration in the arid and semiarid zones of China: Quantified evidence and  
713 implications from satellites. *Land degrad, Dev.*, 29(11), 3841-3851,

714 <https://doi.org/10.1002/ldr.3135>, 2018.

715 Meng, X., Lv, S., Zhang, T., Guo, J., Gao, Y., Bao, Y., Wen, L., Luo, S., and Liu, Y.:  
716 Numerical simulations of the atmospheric and land conditions over the jinta oasis in  
717 northwestern China with satellite-derived land surface parameters, *J. Geophys. Res.-*  
718 *Atmos.*, 114, 605-617, <https://doi.org/10.1029/2008JD010360>, 2009.

719 Potchter, O., Goldman, D., Kadish, D., and Iluz, D.: The oasis effect in an extremely  
720 hot and arid climate: The case of southern Israel, *J. Arid Environ.*, 72, 1721-1733,  
721 <https://doi.org/10.1016/j.jaridenv.2008.03.004>, 2008.

722 Qu, Y. H., Zhu, Y. Q., Han, W. C., Wang, J. D., and Ma, M. G: Crop leaf area index  
723 observations with a wireless sensor network and its potential for validating remote  
724 sensing products, *IEEE J-STARS.*, 7(2), 431-444,  
725 <https://doi.org/10.1109/JSTARS.2013.2289931>, 2014.

726 Scanlon, B. R., Keese, K. E., Flint, A. L., Flint, L. E., Gaye, C. B., Edmunds, W. M.,  
727 and Simmers, I.: Global synthesis of groundwater recharge in semiarid and arid  
728 regions, *Hydrol. Process*, 20 (15), 3335–3370, <https://doi.org/10.1002/hyp.6335>,  
729 2006.

730 Stone, K. B.: Burke-Litwin organizational assessment survey: reliability and validity,  
731 *Organization development journal*, 33(2), 33-50, 2015.

732 Stanev, E., Staneva, J., Bullister, J., and Murray, J.: Ventilation of the black sea  
733 pycnocline. Parameterization of convection, numerical simulations and validations  
734 against observed chlorofluorocarbon data, *Deep sea research part I: Oceanographic*  
735 *research papers*, 51 (12), 2137-2169, <https://doi.org/10.1016/j.dsr.2004.07.018>, 2004.

736 Stoy, P.C., Mauder, M., Foken, T., Marcolla, B., Boegh, E., Ibrom, A., Arain, M., Arneth,  
737 A., Aurela, M., Bernhofer, C., Cescatti, A., Dellwik, E., Duce, P., Gianelle, D., Gorsel,  
738 E., Kiely, G., Knohl, A., Margolis, H., McCaughey, H., Merbold, L., Montagnanti,  
739 L., Papale, D., Reichstein, M., Saunders, M., Serrano-Ortiz, P., Sottocornola, M.,  
740 Spano, D., Vaccari, F., and Varlagin, A: A data-driven analysis of energy balance  
741 closure across FLUXNET research sites: The role of landscape scale heterogeneity,  
742 *Agric. For. Meteorol.*, 171-172, 137-152,  
743 <http://dx.doi.org/10.1016/j.agrformet.2012.11.004>, 2013.

744 Song, L.S., Liu, S.M., Kustas, W.P., Nieto, H., Sun, L., Xu, Z.W., Skaggs, T.H., Yang,  
745 Y., Ma, M.G., Xu, T.R., Tang, X.G., and Li, Q.P.: Monitoring and validating spatially  
746 and temporally continuous daily evaporation and transpiration at river basin scale,  
747 *Remote sens. environ.*, 219, 72-88, <https://doi.org/10.1016/j.rse.2018.10.002>, 2018.

748 Taha, H., Akbari, H., and Rosenfeld, A.: Heat island and oasis effects of vegetative  
749 canopies, *Theor. Appl. Climatol.*, 44, 123-138, <https://doi.org/10.1007/BF00867999>,  
750 1991.

751 Tagesson, T., Fensholt, R., Cappelaere, B., Mougine, E., Horion, S., Kergoat, L., Nieto,  
752 H., Mbow, C., Ehammer, A., Demarty, J., and Ardö, J.: Spatiotemporal variability in  
753 carbon exchange fluxes across the Sahel, *Agric. For. Meteorol.*, 226-227, 108-118,  
754 <https://doi.org/10.1016/j.agrformet.2016.05.013>, 2016.

755 Twine, T.E., Kustas, W.P., Norman, J.M., Cook, D.R., Houser, P.R., Meyers, T.P.,  
756 Prueger, J.H., Starks, P.J., and Wesely, M.L.: Correcting eddy-covariance flux  
757 underestimates over a grassland. *Agric. For. Meteorol.*, 103(3), 279-300,

758 [https://doi.org/10.1016/S0168-1923\(00\)00123-4](https://doi.org/10.1016/S0168-1923(00)00123-4), 2000.

759 Wang, J. M., and Mitsuta, Y.: Evaporation from the desert: some preliminary results of  
760 HEIFE, Boundary Layer Meteorology, 59, 413-418,  
761 <https://doi.org/10.1007/BF0221546>, 1992.

762 Wang, G. X., and Cheng, G. D.: Water resource development and its influence on the  
763 environment in arid areas of China-the case of the Hei River basin, J. Arid Environ.,  
764 43, 121–131, <https://doi.org/10.1006/jare.1999.0563>, 1999.

765 Wang, H. B., Li, X., Xiao, J. F., Ma, M. G., Tan, J. L., Wang, X. F., and Geng, L. Y.:  
766 Carbon fluxes across alpine, oasis, and desert ecosystems in northwestern China: The  
767 importance of water availability, Sci. total environ., 697, 133978,  
768 <https://doi.org/10.1016/j.scitotenv.2019.133978>, 2019.

769 Wen, X., Lv, S., and Jin, J.: Integrating remote sensing data with WRF for improved  
770 simulations of oasis effects on local weather processes over an arid region in  
771 northwestern China, J. Hydrometeorol., 13(2), 573-587,  
772 <https://doi.org/10.1175/JHM-D-10-05001.1>, 2012.

773 Wu, D. X., Liu, S. M., Wu, X. C., Xu, T. R., Xu, Z. W., He, X. L., and Shi, H. Y.:  
774 Evaluation of the intrinsic temperature sensitivity of ecosystem respiration in typical  
775 ecosystems of an endorheic river basin, Agric. For. Meteorol., 333, 109393,  
776 <https://doi.org/10.1016/j.agrformet.2023.109393>, 2023.

777 Xu, Z. W., Liu, S. M., Li, X., Shi, S. J., Wang, J. M., Zhu, Z. L., Xu, T. R., Wang, W.  
778 Z., and Ma, M. G.: Intercomparison of surface energy flux measurement systems  
779 used during the HiWATER-MUSOEXE, J. Geophys. Res.-Atmos., 118, 13140-

780 13157, <https://doi.org/10.1002/2013JD020260>, 2013.

781 Xu, Z.W., Ma, Y.F., Liu, S.M., Shi, W.J., and Wang, J.M.: Assessment of the energy  
782 balance closure under advective conditions and its impact using remote sensing data,  
783 *J. Appl. Meteorol. Clim.*, 56 (1), 127-140, [https://doi.org/10.1175/JAMC-D-16-](https://doi.org/10.1175/JAMC-D-16-0096.1)  
784 0096.1, 2017.

785 Xu, Z. W., Liu, S. M., Zhu, Z. L., Zhou, J., Shi, W. J., Xu, T. R., Yang, X. F., Zhang, Y.,  
786 and He, X.L.: Exploring evapotranspiration changes in a typical endorheic basin  
787 through the integrated observatory network, *Agric. For. Meteorol.*, 290, 108010,  
788 <https://doi.org/10.1016/j.agrformet.2020.108010>, 2020.

789 Xue, J., Gui, D., Lei, J., Sun, H., Zeng, F., Mao, D., Zhang, Z., Jin, Q., and Liu, Y.:  
790 Oasis microclimate effects under different weather events in arid or hyper arid  
791 regions: A case analysis in southern Taklimakan desert and implication for  
792 maintaining oasis sustainability, *Theor. Appl. Climatol.*, 137, 89-101,  
793 <https://doi.org/10.1007/s00704-018-2567-5>, 2019.

794 Zhang, Y. Y., and Zhao, W. Z.: Vegetation and soil property response of short-  
795 timefencing in temperate desert of the Hexi Corridor northwestern China, *Catena*,  
796 133, 43–51, <https://doi.org/10.1016/j.catena.2015.04.019>, 2015.

797 Zhang, X. Y., Arimoto, R., Zhu, G. H., Chen, T., and Zhang, G. Y.: Concentration, size-  
798 distribution and deposition of mineral aerosol over Chinese desert regions, *Tellus B:*  
799 *Chemical and Physical Meteorology*, 50(4), 317-330,  
800 <https://doi.org/10.3402/tellusb.v50i4.16131>, 2016a.

801 Zhang, Q., Sun, R., Jiang, G.Q., Xu, Z. W., and Liu, S. M.: Carbon and energy flux

802 from a *Phragmites australis* wetland in Zhangye oasis-desert area, China, *Agric. For.*  
803 *Meteorol.*, 230-231, 45-57, <https://doi.org/10.1016/j.agrformet.2016.02.019>, 2016b.

804 Zhang, Y., Zhao, W., He, J., and Fu, L.: Soil susceptibility to macropore flow across a  
805 desert-oasis ecotone of the Hexi Corridor, Northwest China, *Water Resour. Res.*, 54,  
806 1281–1294, <https://doi.org/10.1002/2017WR021462>, 2018.

807 Zhang, Z., Poulter, B., Knox, S., Stavert, A., McNicol, G., Fluet-Chouinard, E.,  
808 Feinberg, A., Zhao, Y., Bousquet, P., Canadell, J., Ganesan, A., Hugelius, G., Jackson,  
809 R., Patra, P., Saunio, M., Höglund-Isaksson, L., Huang, C., Chatterjee, A., and Li,  
810 X.: Anthropogenic emission is the main contributor to the rise of atmospheric  
811 methane during 1993–2017, *Natl. Sci. Rev.*, 9(5), nwab200,  
812 <https://doi.org/10.1093/nsr/nwab200>, 2022.

813 Zhang, Y., Liu, S. M., Song, L. S., Li, X., Jia, Z. Z., Xu, T. R., Xu, Z. W., Ma, Y. F.,  
814 Zhou, J., Yang, X. F., He, X. L., Yao, Y. J., and Hu, G. C.: Integrated Validation of  
815 Coarse Remotely Sensed Evapotranspiration Products over Heterogeneous Land  
816 Surfaces, *Remote Sens.*, 14, 3467, <https://doi.org/10.3390/rs14143467>, 2022.

817 Zhao, R., Chen, Y., Shi, P., Zhang, L., Pan, J., and Zhao, H.: Land use and land cover  
818 change and driving mechanism in the arid inland river basin: a case study of Tarim  
819 River, Xinjiang, China, *Environ. Earth sci.*, 68(2), 591-604, <https://doi.org/10.1007/s12665-012-1763-3>, 2013.

821 Zheng, C., Liu, S. M., Song, L. S., Xu, Z. W., Guo, J. X., Ma, Y. F., Ju, Q., and Wang,  
822 J. M.: Comparison of sensible and latent heat fluxes from optical-microwave  
823 scintillometers and eddy covariance systems with respect to surface energy balance

824 closure, *Agric. For. Meteorol.*, 331, 109345,  
825 <https://doi.org/10.1016/j.agrformet.2023.109345>, 2023.

826 Zhou, Y., and Li, X.: Energy balance closures in diverse ecosystems of an endorheic  
827 river basin, *Agric. For. Meteorol.*, 274, 118-131,  
828 <https://doi.org/10.1016/j.agrformet.2019.04.019>, 2018.

829 Zhou, Y., Liao, W., and Li, X.: The contributions of individual factors to the oasis cold  
830 island effect intensity in the Heihe River Basin, *Agric. For. Meteorol.*, 312, 108706,  
831 <https://doi.org/10.1016/j.agrformet.2021.108706>, 2022.